NASA TECHNICAL NOTE

NASA TN D-3887

NASA TN D-3887

LOW SUBSONIC FLIGHT AND FORCE INVESTIGATION OF A SUPERSONIC TRANSPORT MODEL WITH A HIGHLY SWEPT ARROW WING

by Delma C. Freeman, Jr.

Langley Research Center
Langley Station, Hampton, Va.

NATIONAL AERONAUTICS AND SPACE ADMINISTRATION • WASHINGTON, D. C. • JUNE 1967

NASA TN D-3887

LOW SUBSONIC FLIGHT AND FORCE INVESTIGATION OF A SUPERSONIC TRANSPORT MODEL WITH A HIGHLY SWEPT ARROW WING

By Delma C. Freeman, Jr.

Langley Research Center
Langley Station, Hampton, Va.

Technical Film Supplement L-949 available on request.

NATIONAL AERONAUTICS AND SPACE ADMINISTRATION

For sale by the Clearinghouse for Federal Scientific and Technical Information
Springfield, Virginia 22151 – CFSTI price $3.00

LOW SUBSONIC FLIGHT AND FORCE INVESTIGATION OF A SUPERSONIC TRANSPORT MODEL WITH A HIGHLY SWEPT ARROW WING

By Delma C. Freeman, Jr.
Langley Research Center

SUMMARY

An investigation has been conducted in the Langley full-scale tunnel to determine the low-speed static and dynamic longitudinal and lateral stability characteristics of a model of a highly swept, blended-wing-body, supersonic commercial air transport configuration. The model was tested in its basic configuration and with several different modifications. The flight tests were conducted over an angle-of-attack range from about 6° to 30°. Static and dynamic force tests were conducted at angles of attack from -3° to 37°.

The results of the static force tests showed that the basic configuration had severe longitudinal instability in the form of a pitch-up at an angle of attack of about 10°, but that the point at which instability occurred could be shifted to an angle of attack of 25° by the use of several geometric modifications. In this modified configuration (canard surface off), the model had satisfactory longitudinal flight characteristics at the low angles of attack but the longitudinal stability decreased with increasing angle of attack. The longitudinal control power was somewhat weak for maneuvering and recovering from disturbances and it became weaker with increasing angle of attack. The directional stability was satisfactory, but the Dutch roll oscillation was lightly damped throughout the test angle-of-attack range. The use of a rate damper to provide artificial stabilization in roll generally gave satisfactory Dutch roll characteristics. The lateral control of the configuration was adequate at low angles of attack but decreased with increasing angle of attack and became very weak at an angle of attack of about 20°. The addition of a high-lift canard surface as part of a high lift system permitted an increase in lift coefficient of 0.1 in the angle-of-attack range for take-off and landing. This canard surface had no effect on the dynamic longitudinal stability except that it required about a 0.03 mean aerodynamic chord forward shift in the center of gravity to achieve the same longitudinal stability as the canard-off configuration. The addition of the canard surface also decreased the Dutch roll damping and at an angle of attack of about 20° with the canard surface on, the oscillation was unstable.

INTRODUCTION

For the past few years, the National Aeronautics and Space Administration has been conducting an extensive research effort in support of a supersonic transport program to obtain a satisfactory configuration for best performing specified mission requirements. As part of this general study, the Langley Research Center has conducted an investigation in the Langley full-scale tunnel to determine the low-speed static and dynamic stability characteristics of a model of a highly swept blended-wing-body supersonic commercial air transport configuration which has been designated SCAT-15F. This configuration, which is described in reference 1, has a twisted and cambered arrow wing and makes use of favorable interference effects to give high aerodynamic efficiency in supersonic flight as reported in reference 2. The results presented in reference 2 showed that the high-speed performance of the SCAT-15F was very favorable, but preliminary work at low speeds, corresponding to the take-off and landing phases of flight, showed that the configuration had severe static longitudinal instability, or pitch-up, at a relatively low angle of attack. Considerable effort, both in this investigation and in an investigation reported in reference 3, has been directed toward the achievement of satisfactory low-speed longitudinal stability characteristics through various modifications to the basic design.

The present investigation consisted of free-flight tests, static and dynamic force tests, and dynamic lateral stability calculations.

SYMBOLS

The longitudinal data are referred to the stability system of axes and the lateral data are referred to the body system of axes. (See fig. 1.) The origin of the axes was located to correspond to the center of gravity shown in figure 2.

In order to facilitate international usage of data presented, dimensional quantities are presented in both U.S. Customary Units and in the International System of Units (SI). The equivalent dimensions were determined in each case by using the conversion factors given in reference 4.

b	wing span, ft (cm)
$\bar{c}$	mean aerodynamic chord, ft (cm)
$1/C_{1/2}$	inverse cyclic damping
C_A	axial-force coefficient, $F_A/q_\infty S$

$$C_{A_q} = \frac{\delta C_A}{\delta \frac{q\bar{c}}{2V}}$$

$$C_{A_{\dot{\alpha}}} = \frac{\delta C_A}{\delta \frac{\dot{\alpha}\bar{c}}{2V}}$$

C_D drag coefficient, $F_D/q_\infty S$

C_l rolling-moment coefficient, $M_X/q_\infty Sb$

ΔC_l incremental rolling-moment coefficient

$$C_{l_p} = \frac{\partial C_l}{\partial \frac{pb}{2V}}$$

$$C_{l_r} = \frac{\partial C_l}{\partial \frac{rb}{2V}}$$

$C_{l_\beta} = \frac{\partial C_l}{\partial \beta}$ per degree or per radian

$$C_{l_{\dot{\beta}}} = \frac{\partial C_l}{\partial \frac{\dot{\beta}b}{2V}}$$

C_L lift coefficient, $F_L/q_\infty S$

C_m pitching-moment coefficient, $M_Y/q_\infty S\bar{c}$

$$C_{m_q} = \frac{\delta C_m}{\delta \frac{q\bar{c}}{2V}}$$

$$C_{m_{\dot{\alpha}}} = \frac{\delta C_m}{\delta \frac{\dot{\alpha}\bar{c}}{2V}}$$

C_n yawing-moment coefficient, $M_Z/q_\infty Sb$

ΔC_n incremental yawing-moment coefficient

$$C_{n_p} = \frac{\partial C_n}{\partial \frac{pb}{2V}}$$

$$C_{n_r} = \frac{\partial C_n}{\partial \frac{rb}{2V}}$$

$$C_{n_\beta} = \frac{\partial C_n}{\partial \beta} \text{ per degree or per radian}$$

$$C_{n_{\dot\beta}} = \frac{\partial C_n}{\partial \frac{\dot\beta b}{2V}}$$

C_N normal-force coefficient, $F_N/q_\infty S$

$$C_{N_q} = \frac{\delta C_N}{\delta \frac{q\bar{c}}{2V}}$$

$$C_{N_{\dot\alpha}} = \frac{\delta C_N}{\delta \frac{\dot\alpha \bar{c}}{2V}}$$

C_Y side-force coefficient, $F_Y/q_\infty S$

ΔC_Y incremental side-force coefficient

$$C_{Y_p} = \frac{\partial C_Y}{\partial \frac{pb}{2V}}$$

$$C_{Y_r} = \frac{\partial C_Y}{\partial \frac{rb}{2V}}$$

$$C_{Y_\beta} = \frac{\partial C_Y}{\partial \beta} \text{ per degree or per radian}$$

$$C_{Y_{\dot{\beta}}} = \frac{\partial C_Y}{\partial \frac{\dot{\beta} b}{2V}}$$

e_1 control surface located between nacelles (fig. 3(a))

e_2 control surface just outboard of nacelles (fig. 3(a))

e_3 control surface located outboard of vertical tail (fig. 3(a))

e_4 flap located between inboard nacelle and fuselage (fig. 3(a))

f frequency of oscillations, cps

F_A axial force, lb (N)

F_D drag force, lb (N)

F_L lift force, lb (N)

F_N normal force, lb (N)

F_Y lateral force, lb (N)

I_X moment of inertia about longitudinal body axis, slug-ft^2 (kg-m^2)

I_Y moment of inertia about lateral body axis, slug-ft^2 (kg-m^2)

I_Z moment of inertia about normal body axis, slug-ft^2 (kg-m^2)

k reduced-frequency parameter, $\omega b/2V$ or $\omega \bar{c}/2V$

L/D lift-drag ratio

m mass, slug (kg)

M_X rolling moment, ft-lb (N-m)

M_Y pitching moment, ft-lb (N-m)

M_Z yawing moment, ft-lb (N-m)

p rolling velocity, radians/sec

P period, sec

q pitching velocity, radians/sec

q_∞ dynamic pressure, lb/ft^2 (N/m^2)

r yawing velocity, radians/sec

R Reynolds number based on mean aerodynamic chord

S wing area, ft^2 (cm^2)

t time, sec

$t_{1/2}$ time to damp to half-amplitude, sec

$v_e = V\sqrt{\sigma} \sin \beta \approx V\sqrt{\sigma}\beta$

V free-stream velocity, ft/sec (m/sec)

X,Y,Z body reference axes unless otherwise noted

α angle of attack, deg or radians

$\dot{\alpha}$ rate of change of angle of attack, radians/sec

β angle of sideslip, deg or radians

$\dot{\beta}$ rate of change of angle of sideslip, radians/sec

δ_a total aileron deflection, $\delta_{e,L} - \delta_{e,R}$, deg

δ_e elevator deflection, positive when trailing edge is down, deg

$\delta_{e,L}$ left elevon deflection, positive when trailing edge is down, deg

$\delta_{e,R}$ right elevon deflection, positive when trailing edge is down, deg

δ_n leading-edge flap deflection, positive when leading edge is up, deg

δ_r deflection of each rudder, positive when trailing edge is deflected to left, deg

μ relative-density factor, $m/\rho Sb$

ρ air density, slug/ft^3 (kg/m^3)

σ ratio of air density at altitude to that at sea level

ϕ angle of roll, radians

$\left|\frac{\phi}{v_e}\right|$ ratio of bank-angle amplitude to equivalent side-velocity amplitude for oscillatory mode, $\left|\frac{\phi}{\beta}\right|\frac{57.3}{V\sqrt{\sigma}}$, deg/ft/sec (deg/m/sec)

ψ angle of yaw, radians

ω angular velocity, $2\pi f$, radians/sec

Subscript:

s denotes stability axes

APPARATUS AND MODEL

A drawing of the model used in the investigation is presented in figure 2, and the mass and dimensional characteristics of the model are presented in table I. The model had an arrow planform wing with 74° leading-edge sweep, twin outboard vertical tails, and four nacelles located under the wing. The two most outboard wing trailing-edge control surfaces (e_2 and e_3) were used for longitudinal trim and control. (See fig. 3(a).) Lateral directional control was obtained by using these same surfaces and the two rudders. The model was provided with several different modifications which were designed

to minimize the static longitudinal instability of the basic configuration. These modifications, which are shown in figures 2 and 3, included a larger leading-edge radius, leading-edge flaps, a trailing-edge extension, a wing apex notch, two different canard surfaces, wing fences, and wing leading-edge slats. The wing leading-edge radius noted in figure 2 is that of the larger leading-edge radius; in the original configuration the wing had a sharp leading edge.

The flight tests were made in the Langley full-scale tunnel, and a sketch of the flight test equipment and setup is given in figure 4. A description of the flight test equipment and setup is given in reference 5. A photograph of the model flying in the tunnel is presented in figure 5(a). All force tests were made in the Langley full-scale tunnel with a sting support system and internal strain-gage balances. A photograph of the model mounted for the static force tests is shown in figure 5(b). Longitudinal oscillation tests using the forced oscillation technique were made on an apparatus described in reference 6. Lateral oscillation tests using the same technique were made on an apparatus similar to the one described in reference 7, except that an automatic readout system was employed.

TESTS

Flight Tests

The flight tests were made to determine the dynamic stability and control characteristics and the general flight behavior of the model. The model behavior during flight was observed by the pitch pilot (located at the side of the test section) and by the yaw and roll pilot (located in the rear of the test section). (See fig. 4.) The results obtained in the flight tests were primarily in the form of qualitative ratings of the flight behavior based on pilots' opinions. Motion-picture records were obtained in the tests for subsequent study and to verify and correlate the ratings for the different flight conditions. Flight tests were made with the model employing several of the modifications which appeared most effective in achieving satisfactory static longitudinal stability. For simplicity, the flight test results are discussed in terms of the canard-off and canard-on configurations. The canard-off configuration consisted of the basic model plus the increased leading-edge radius, the trailing-edge extension, the wing apex notch, and the leading-edge flaps deflected downward 45°. (See fig. 3(a).) The canard-on configuration employed all the modifications of the canard-off configuration plus the 2-percent high-lift canard surface shown in figure 3(c). The canard surface was regarded mainly as means of trimming model with trailing-edge flaps deflected for high lift; and canard-on tests were made only with flaps of the canard surface deflected 54° as shown in figure 3(c).

The model was flown over an angle-of-attack range from 6° to 30°. For most of the flights, the center of gravity was located at $0.42\bar{c}$ (9-percent static margin) for the canard-off configuration, and at $0.37\bar{c}$ (10-percent static margin) for the canard-on configuration. The effect of the center-of-gravity location was determined in flights at an angle of attack of about 13° for both configurations. The control deflections used in most of the flight tests were $\pm 10^{\circ}$ for elevator, $\pm 12^{\circ}$ on each rudder for directional control, and $\pm 11^{\circ}$ on each aileron for roll control. In some flights, a roll damper using a rate gyro as the sensing element was used to provide artificial damping in roll.

Force Tests

Static and dynamic force tests were made to determine the static stability and control characteristics and the dynamic stability derivatives of the model for correlation with the flight test results. These force tests were conducted for the basic configuration and for the modified configurations.

The static and dynamic force tests generally were made over an angle-of-attack range from -3° to 30°. The static lateral stability characteristics were determined both from the incremental differences in C_n, C_l, and C_Y measured at fixed angles of sideslip over an angle-of-attack range, and from measurements over a sideslip range at fixed angles of attack. The dynamic longitudinal stability derivatives were measured for an amplitude of ± 0.134 radian and for a frequency of 0.4 cycle per second, which corresponds to a value of the reduced-frequency parameter k of 0.091. The dynamic lateral stability derivatives were measured for an amplitude of ± 0.087 radian in both roll and yaw for a frequency of 0.8 cycle per second, which corresponds to a value of k of 0.332.

The force tests were conducted over a range of dynamic pressures from 2.15 lb/ft^2 (102.9 N/m^2) to 4.06 lb/ft^2 (194.0 N/m^2) which corresponds to a range of Reynolds numbers from 1.10×10^6 to 1.51×10^6. The model was so small in proportion to the tunnel test section that no wind-tunnel corrections were needed or made.

Calculations

Linear three-degree-of-freedom lateral stability equations were used to calculate the period and damping of the Dutch roll oscillation and the damping of the lateral aperiodic modes for both the canard-off and canard-on configurations. These calculations were made with the use of the stability derivatives measured in the force-test part of this investigation. The effect on the lateral period and damping characteristics was also determined for large changes in the damping-in-roll derivative $C_{l_p} + C_{l_\beta} \sin \alpha$ such as might be achieved by the use of artificial damping in roll. In addition, the

roll-velocity—side-velocity parameter ϕ/v_e and the inverse cyclic damping $1/C_{1/2}$ were determined and the results were compared with the handling qualities requirement of reference 8.

FORCE-TEST RESULTS AND DISCUSSION

Longitudinal Stability and Control Characteristics

The static longitudinal stability data for the basic model are presented in figure 6. Also presented in this figure are higher Reynolds number data for comparison purposes. These data show that Reynolds number had little effect on the pitching-moment characteristics but did have some significant effect on the lift and drag characteristics, the higher Reynolds number data showing, as expected, a higher maximum value of L/D. The data show that the configuration had static longitudinal stability at low positive angles of attack but had an unstable break in the pitching-moment curve at an angle of attack of about 10°, and severe longitudinal instability at the higher angles of attack. This severe instability is attributed to the combined effects of the cranked wing tips, the trailing-edge cutout, and, to some extent, the sharp leading edge of the wing.

Considerable work has been done in both this investigation and the investigation reported in reference 3 to alleviate the longitudinal instability. One modification which proved to be beneficial in delaying the onset of static longitudinal instability was the use of leading-edge flaps. The data of figure 7 show that the use of leading-edge flaps gave stability for angles of attack up to 20°. These data also show that the results of the present investigation are in agreement with higher Reynolds number data. The higher Reynolds number data have also indicated that an increase in leading-edge radius delayed the onset of longitudinal instability. Consequently, the increased leading-edge radius was tested in the present investigation, and data showing the effect of leading-edge radius on the longitudinal stability characteristics of the model with leading-edge flaps deflected downward 30° is presented in figure 8. Since the data show a slight delay in the onset of longitudinal instability and a decrease in the instability at high angles of attack, the increased leading-edge radius was employed on the model for all subsequent tests, and all the remaining data presented herein are for the case of increased leading-edge radius. Other modifications which were studied in the present investigation included fences, leading-edge slats, a trailing-edge extension, and a wing apex notch. Results of tests with fences and leading-edge slats on the model (fig. 9) indicate that these devices had little effect on the pitching-moment characteristics. Two of the more effective modifications studied were a trailing-edge extension and a wing apex notch. Data showing the effect of these modifications on the longitudinal characteristics of the model are shown in figures 10 and 11. These data show that the wing trailing-edge

extension had little effect on the longitudinal stability characteristics at low and moderate angles of attack but did reduce the magnitude of the instability at the higher angles of attack. The addition of the wing apex notch increased the stability at low angles of attack and appreciably reduced the instability at the higher angles.

Presented in figure 12 are data showing the effect of the trailing-edge extension and notch used in conjunction with leading-edge flaps. The data show that the beneficial effects of these modifications tended to be additive, and the stability characteristics of the model with this combination of devices were the most promising achieved in the present investigation. This configuration was therefore selected for flight tests as the canard-off configuration and is referred to as such in the remainder of the report. In this configuration the model was stable for angles of attack up to 16°, neutrally stable at angles between 16° and 25°, and unstable at angles of attack above 25°.

One adverse effect of the foregoing modifications is that they appreciably reduced the lift-curve slope; and this reduction in lift-curve slope is detrimental to the take-off and landing performance. The variable-geometry canard surfaces were therefore tested as a device which would make it possible to provide pitching moment for trim with the trailing-edge flaps deflected downward to produce more lift. These canard surfaces also provided the additional benefit of reducing the longitudinal instability at high lift coefficients. Presented in figure 13 are the results obtained with the 5-percent canard surface tested in this investigation compared with higher Reynolds number data. The data in both cases show that the canard surface was destabilizing at low angles of attack, but that it did reduce the magnitude of instability at the higher angles. The data of the present investigation agree very well with the higher scale data. Figure 14 presents data obtained by using the 2-percent high-lift canard surface which employed leading-edge slats and double slotted trailing-edge flaps. (See fig. 3(c).) The canard was tested in conjunction with the trailing-edge extension, wing apex notch, and the leading-edge flaps deflected downward 45°. The results of these tests, presented in figure 14, show that the model in this configuration had static longitudinal stability up to an angle of attack of about 25°, but that the use of the canard surface moved the aerodynamic center about 3 percent forward and would require a corresponding forward shift in the center of gravity to give the same stability as the canard-off configuration. This configuration was flight tested as the canard-on configuration and is referred to as such in the remainder of the report. The data of figure 14 also show that the high-lift canard surface provided a positive pitching moment which could be used for trimming out the diving moment of a trailing-edge wing flap.

The elevator effectiveness for the canard-off and canard-on configurations is presented in figures 15(a) and 15(b), respectively. The control effectiveness was constant for angles of attack up to about 25° and was sufficient for both configurations to trim the

model over the range for which the model had longitudinal stability. The data of figure 15(b) show that the high-lift canard surface provided enough positive pitching moment to trim out the diving moments associated with a downward deflection of about 10° on the wing trailing-edge surfaces. The use of this particular canard surface in this manner resulted in an increase in trim lift coefficient of about 0.10 over the entire range of angles of attack for which the model was longitudinally stable. One significant point noted in the data of figure 15(b) is that the downward deflection of the two inboard surfaces e_1 and e_4 proved detrimental to the stability of the configuration in that a destabilizing break occurred in the pitching-moment curve at a relatively low angle of attack and the instability at the higher angles of attack became more severe. The reason for this unstable break is not known, but it may be associated with flow separation induced near the wing-fuselage juncture when the surface e_4 was deflected.

The oscillatory stability derivatives measured in the pitching oscillation tests are presented in figure 16. These data show that both the canard-off and the canard-on configurations have positive damping in pitch $\left(\text{negative values of } C_{m_q} + C_{m_{\dot{\alpha}}}\right)$ over the test angle-of-attack range.

Lateral Stability and Control Characteristics

The basic static lateral stability data for the canard-off and canard-on configurations are presented in figures 17 and 18. The data of figure 17 show that the variations of C_Y, C_n, and C_l with changes in sideslip were linear over the test angle-of-attack range for both the canard-off and canard-on configurations. The data presented in figure 18 determined from the incremental differences in C_l, C_n, and C_Y measured over the angle-of-attack range at sideslip angles of 5° and -5° show that the configurations were directionally stable $\left(+C_{n_\beta}\right)$ and had positive dihedral effect $\left(-C_{l_\beta}\right)$ throughout the test angle-of-attack range.

The aileron effectiveness data are presented in figure 19. These data show that the effectiveness was approximately constant for angles of attack up to about 10° but decreased as the angle of attack was increased above this value. The yawing moment produced by aileron deflection was very small throughout the angle-of-attack range.

The rudder effectiveness data for the canard-off and canard-on configurations are presented in figure 20. These data show that the rudder effectiveness decreased with increasing angle of attack.

The lateral oscillatory derivatives measured in yawing and rolling tests are presented in figure 21. The data show that the model had positive damping in roll and positive damping in yaw over the entire angle-of-attack range and that $C_{n_r} - C_{n_{\dot{\beta}}} \cos \alpha$ was

substantially higher, and $C_{l_p} + C_{l_{\dot{\beta}}} \cos \alpha$ somewhat lower, at the high angles of attack with the canard surface on.

FLIGHT-TEST RESULTS AND DISCUSSION

A motion-picture film supplement covering the flight tests of the model has been prepared and is available on loan. A request card form and a description of the film are found at the end of the report.

Longitudinal Stability and Control Characteristics

Canard off.- The longitudinal stability characteristics of the canard-off configuration were found to be generally satisfactory in the angle-of-attack range from 6° to 15° for the design center-of-gravity position of $0.45\bar{c}$. The model was longitudinally stable and could be flown steadily. It was affected much less by turbulence in the tunnel airstream than other models tested in the past. This characteristic probably resulted from the fact that the model had low lift-curve slope, low static longitudinal stability, and high pitching moment of inertia. The control power was somewhat weak for maneuvering or for correcting for disturbances. The principal reason for the weakness of the control was probably that the control surfaces were rather small and thus produced only about 40 to 50 percent as much pitching-moment coefficient per degree of control deflection as the controls of other highly swept tailless airplane configurations tested in the past. The pitch control became progressively weaker as the angle of attack was increased because of the reduction in dynamic pressure.

As the angle of attack was increased above 15°, there was a noticeable reduction in the longitudinal stability and control effectiveness which caused the model to become increasingly more difficult to fly. Flights could be made fairly easily as long as the motions remained relatively small, but the pilot had little authority over the model from the standpoint of maneuvering or correcting disturbances. At angles of attack near 22°, the model was very difficult to fly because of static longitudinal instability and weak longitudinal control and most flights ended with the model pitching up against full corrective control.

As part of the flight-test investigation, tests were made to determine the effect of static margin on the longitudinal flight characteristics of the model. These tests were made at an angle of attack of about 13°. The results of these tests showed that the model had good longitudinal stability characteristics and adequate control with the center of gravity in the range from $0.42\bar{c}$ to $0.48\bar{c}$ (9- to 3-percent static margin). There was, however, a slight progressive deterioration in both longitudinal stability and control characteristics as the center of gravity was moved rearward. When the center of gravity

was moved rearward to $0.50\bar{c}$ (1-percent static margin), the model was unsteady longitudinally and was very sensitive to control inputs and gust disturbances and required constant attention of the pilot to maintain flight. This condition seemed more difficult to fly than would normally be expected just on the basis of the low static margin. The flight difficulty with near neutral stability is probably associated with the high pitch inertia and weak longitudinal control which made recovery from disturbances very slow.

Canard on.- The longitudinal flight behavior of the canard-on configuration was found to be generally similar to that of the canard-off configuration when the center of gravity was moved forward 3 percent to $0.42\bar{c}$ to offset the destabilizing effect of the canard. At angles of attack from 7° to 15°, the model was stable and flew steadily and was very easy to fly even though the control was somewhat weak, as was the case for the canard-off configuration. Increasing the angle of attack above 15° resulted in a marked deterioration in longitudinal flight behavior because of reduced longitudinal stability and control. An angle of attack of about 17° was considered to be about the highest at which the flight behavior was generally acceptable. At angles of attack slightly above this value, the stability and control characteristics deteriorated to the point where sustained flights were extremely difficult, but with careful attention to control, the model was flown up to an angle of attack of about 22°. At this condition any disturbance which caused the model to pitch away from its trim attitude generally led to loss of control, and the model diverged in pitch. The use of 1-inch chord extensions on the elevons to increase the control effectiveness at the higher angles of attack generally made sustained flights possible where previously they had been extremely difficult.

The high-lift canard surface permitted the model to be trimmed to an angle of attack of 30°, but at this high angle of attack, it was very longitudinally unstable with a normal center-of-gravity location. As a matter of research interest, however, the center of gravity was moved forward an additional 5 percent of the mean aerodynamic chord (center of gravity at $0.37\bar{c}$) so that the model could be flown in the high angle-of-attack range. With this center-of-gravity location, smooth sustained flights could be made at angles of attack near 20°, but the control was considered too weak for satisfactory control of the model. Increasing the angle of attack to 25° resulted in a reduction in stability and control, but sustained flights were possible with careful attention to control. At an angle of attack of 30°, the model was felt to be about neutrally stable. Sustained flights were made at this angle of attack but the longitudinal control was extremely weak and required the pilot to give maximum attention to control to keep the model flying.

Flight tests to determine the effect of center-of-gravity location on the longitudinal flight characteristics of the canard-on configuration were made at an angle of attack of 13°. The results showed that the model had good longitudinal stability characteristics and adequate control in the center-of-gravity range from 0.37- to 0.45-percent mean

aerodynamic chord (10- to 2-percent static margin). There was, however, a deterioration in the longitudinal stability and control characteristics as the center of gravity was moved rearward. Moving the center of gravity 2 percent further rearward (zero static margin) resulted in a condition that was extremely difficult to fly; and moving the center of gravity one more percent (1-percent negative static margin) resulted in a condition that was almost unflyable. As pointed out earlier, the flight difficulty at this aft center-of-gravity position was probably associated with the weak longitudinal control.

Lateral Stability and Control Characteristics

Canard off.- In brief, the flight tests showed that the canard-off configuration without stability augmentation had satisfactory directional stability but low Dutch roll damping over the test angle-of-attack range. The tests also showed that the model had adequate lateral control at low angles of attack, but that the lateral control characteristics deteriorated with increasing angle of attack. Specifically, at the lowest test angle of attack ($\alpha = 6^{\circ}$), the lateral control was adequate for overcoming disturbances and for maneuvering the model within the limited area of the tunnel airstream. Smooth flights could be made about as well with ailerons alone as with simultaneous use of ailerons and rudder, apparently because of the proverse (favorable) yaw of the ailerons. As the angle of attack was increased, the lateral control deterioration and the Dutch roll damping decreased. At angles of attack near 15°, the model oscillated in roll almost continuously in reponse to the gustiness of the tunnel airflow and the application of corrective control. The directional stability was satisfactory and, although the lateral control was felt to be somewhat sluggish, it was not difficult to keep the model flying within the confines of the tunnel with coordinated aileron and rudder control. Flights with ailerons alone, however, were generally unsuccessful at this angle of attack because such control was inadequate for overcoming large disturbances. Increasing the angle of attack to about 20° resulted in a condition that was difficult to fly, mostly because of low Dutch roll damping and weak lateral control. The directional stability was good, however, and, as long as careful attention was given to control, it was possible to make sustained flights up to the angle of attack at which pitch divergence occurred ($\alpha = 22^{\circ}$). The addition of 1-inch chord extensions to the elevons greatly improved the aileron effectiveness and made control of the model much easier at the higher angles of attack.

The use of a roll rate damper to provide artificial stabilization in roll gave satisfactory Dutch roll damping over the test angle-of-attack range. With the rate damper operating, the lateral flight characteristics were considered to be generally satisfactory except for the weak lateral control at the higher angles of attack.

Presented in figure 22 are period and damping characteristics of the Dutch roll oscillation for the full-scale configuration. These results show that the Dutch roll

oscillation was stable over the test angle-of-attack range for the canard-off configuration. There was a rapid reduction in damping with increase in angle of attack up to an angle of 15°. At an angle of attack of about 15°, the Dutch roll oscillation required about 25 seconds (or, about 4.5 cycles) to damp to one-half amplitude. These results indicate low Dutch roll damping and are generally in good agreement with the flight test results.

In order to show a comparison of the calculated Dutch roll damping of this configuration with the military specifications for flying qualities of piloted airplanes (see ref. 8), the calculated data of figure 22 have been replotted in figure 23(a) in terms of the inverse cyclic damping $1/C_{1/2}$ and the roll-velocity—side-velocity ratio $|\phi/v_e|$. The upper boundary in this plot specifies the value of $1/C_{1/2}$ required for satisfactory Dutch roll damping. The results of this figure show that the damping without stability augmentation was unacceptable for normal operation over the test angle-of-attack range. The plot also shows that the use of a roll rate damper was very effective for increasing the lateral damping and providing satisfactory Dutch roll characteristics.

The calculated roll response data (single degree of freedom) of figure 24 indicate that the ailerons were capable of producing a roll angle of about 8° in 3/4 second at an angle of attack of 8°. Although these calculations are limited in scope, comparison with unpublished three-degree-of-freedom response calculations shows that the two sets of data are in agreement for the time period presented. As the angle of attack was increased, the control response decreased rapidly and at an angle of attack of about 22°, the ailerons produced only about 2.5° of roll in 3/4 second. Flight tests showed the lateral response to be generally satisfactory at angles of attack near 8° but at high angles of attack the response was considered by the pilot to be much too low for satisfactory control of the model.

Canard on.- The flight characteristics of the canard-on configuration were found to be generally similar to those of the canard-off configuration except that the addition of the canard surface appreciably reduced the Dutch roll damping. This result is illustrated clearly by the calculated period and damping data of figure 22, which show that the canard-on configuration had negative values of $1/t_{1/2}$ (unstable damping) over a large part of the test angle-of-attack range. This adverse effect of the canard is primarily associated with the fact that the canard surface reduced the damping in roll of the model, especially at the higher angles of attack as shown in figure 21.

The Dutch roll instability was generally characterized by a pure rolling motion about the X-body axis. When the amplitude of the oscillation was allowed to build up, it generally reached some constant value and the model would fly with this constant-amplitude rolling motion (limit-cycle oscillation) until corrective control was applied. At angles of attack above about 20°, corrective control had little or no effect on this rolling motion and the amplitude of the oscillation reached values as large as $\pm 30^{\circ}$.

The main reason that the model could be flown up to high angles of attack, despite the poor Dutch roll damping, was that the directional stability was good. Even though the model was oscillating in roll the lateral pilot had little difficulty maintaining a heading and keeping the model from diverging in yaw. The lateral control was adequate for flying the model in the low angle-of-attack range, but as in the case of the canard-off configuration, the control decreased rapidly with increasing angle of attack and became sluggish at an angle of attack of about 20°. The use of 1-inch chord extensions to the elevons increased the control effectiveness enough to allow flights to be made to angles of attack as high as 30°, but the control at this angle was so weak that sustained flights were just barely possible.

Although the Dutch roll damping was very poor without artificial stabilization, it was found that satisfactory damping could be achieved through the use of a roll-rate damper to provide artificial stabilization in roll. With the damper on, flights were made over an angle-of-attack range from about 6° up to 30° and the flight characteristics were found to be generally satisfactory except for weak lateral control at the high angles of attack.

A comparison of the calculated Dutch roll damping characteristics of the canard-on configuration with the military specifications for flying qualities of piloted airplanes is shown in figure 23(b). The results of this figure show that, although the configuration had unsatisfactory Dutch roll damping over the test angle-of-attack range without artificial stabilization, the use of a roll-rate damper was effective in providing satisfactory Dutch roll damping characteristics.

CONCLUSIONS

From the force and flight test investigation to determine the low-speed stability and control characteristics of a model of a highly swept supersonic transport configuration, the following conclusions were drawn:

1. The basic configuration had severe static longitudinal instability in the form of a pitch-up at an angle of attack of 10°. Through various modifications, this instability was alleviated or delayed to an angle of attack of about 25°. In this modified configuration with the canard surface off, the model had satisfactory longitudinal flight characteristics at low angles of attack but the longitudinal stability decreased with increasing angle of attack and the model pitched up against corrective control at an angle of attack of about 22°. The longitudinal control power was somewhat weak for maneuvering and recovering from disturbances at the lower angles of attack and it became weaker with increasing angle of attack.

2. The directional stability was satisfactory, but the Dutch roll oscillation was lightly damped throughout the test angle-of-attack range. The use of a roll rate damper to provide artificial stabilization in roll generally gave satisfactory Dutch roll characteristics.

3. The lateral control of the configuration was adequate at low angles of attack but decreased with increasing angle of attack and became very weak at an angle of attack of about 20°.

4. The use of the high-lift canard surface permitted trim with downward deflection of the wing trailing-edge flaps and thereby resulted in an increase in lift coefficient of 0.1 in the angle-of-attack range for take-off and landing. The canard surface had no effect on the dynamic longitudinal stability except it required about a 0.03 mean aerodynamic chord forward shift in the center of gravity to provide the same static longitudinal stability as the canard-off configuration. The canard surface also decreased the Dutch roll damping and at an angle of attack of about 20° the oscillation was unstable with the roll damper off.

Langley Research Center,
National Aeronautics and Space Administration,
Langley Station, Hampton, Va., February 7, 1967,
720-01-00-08-23.

REFERENCES

1. Morris, Odell A.; and Fournier, Roger H.: Aerodynamic Characteristics at Mach Numbers 2.30, 2.60, and 2.96 of a Supersonic Transport Model Having a Fixed, Warped Wing. NASA TM X-1115, 1965.

2. Morris, Odell A.; and Patterson, James C., Jr.: Transonic Aerodynamic Characteristics of Supersonic Transport Model With a Fixed, Warped Wing Having 74° Sweep. NASA TM X-1167, 1965.

3. Henderson, William P.: Low-Speed Aerodynamic Characteristics of a Supersonic Transport Model With a Highly Swept, Twisted and Cambered, Fixed Wing. NASA TM X-1249, 1966.

4. Mechtly, E. A.: The International System of Units – Physical Constants and Conversion Factors. NASA SP-7012, 1964.

5. Paulson, John W.; and Shanks, Robert E.: Investigation of Low-Subsonic Flight Characteristics of a Model of a Hypersonic Boost-Glide Configuration Having a 78° Delta Wing. NASA TN D-894, 1961. (Supersedes NASA TM X-201.)

6. Chambers, Joseph R.; and Grafton, Sue B.: Static and Dynamic Longitudinal Stability Derivatives of a Powered 1/9-Scale Model of a Tilt-Wing V/STOL Transport. NASA TN D-3591, 1966.

7. Hewes, Donald E.: Low-Subsonic Measurements of the Static and Oscillatory Lateral Stability Derivatives of a Sweptback-Wing Airplane Configuration at Angles of Attack From -10° to 90°. NASA MEMO 5-20-59L, 1959.

8. Anon.: Flying Qualities of Piloted Airplanes. Military Specification MIL-F-8785(ASG), Sept. 1, 1954; Amendment-4, Apr. 17, 1959.

TABLE I.- DIMENSIONS AND MASS CHARACTERISTICS OF MODEL

Weight:		
Canard off	49 lb	(218 N)
Canard on	49.5 lb	(220 N)
Wing loading	2.82 lb/ft^2	(135 N/m^2)
Moment of inertia about Z-axis I_Z:		
Canard off	10.08 slug-ft^2	(13.65 kg-m^2)
Canard on	10.70 slug-ft^2	(14.51 kg-m^2)
Moment of inertia about X-axis I_X:		
Canard off	1.35 slug-ft^2	(1.83 kg-m^2)
Canard on	1.44 slug-ft^2	(1.95 kg-m^2)
Moment of inertia about Y-axis I_Y:		
Canard off	8.94 slug-ft^2	(12.11 kg-m^2)
Canard on	9.09 slug-ft^2	(12.32 kg-m^2)
Relative density factor, μ	6.90	
Wing:		
Area	17.38 ft^2	(16 140 cm^2)
Span	5.46 ft	(165.2 cm)
Aspect ratio	1.72	
Mean aerodynamic chord	4.24 ft	(129.2 cm)
Root chord	7.4 ft	(226.0 cm)
Tip chord	0.33 ft	(10.05 cm)
Sweep of leading edge	74^o	

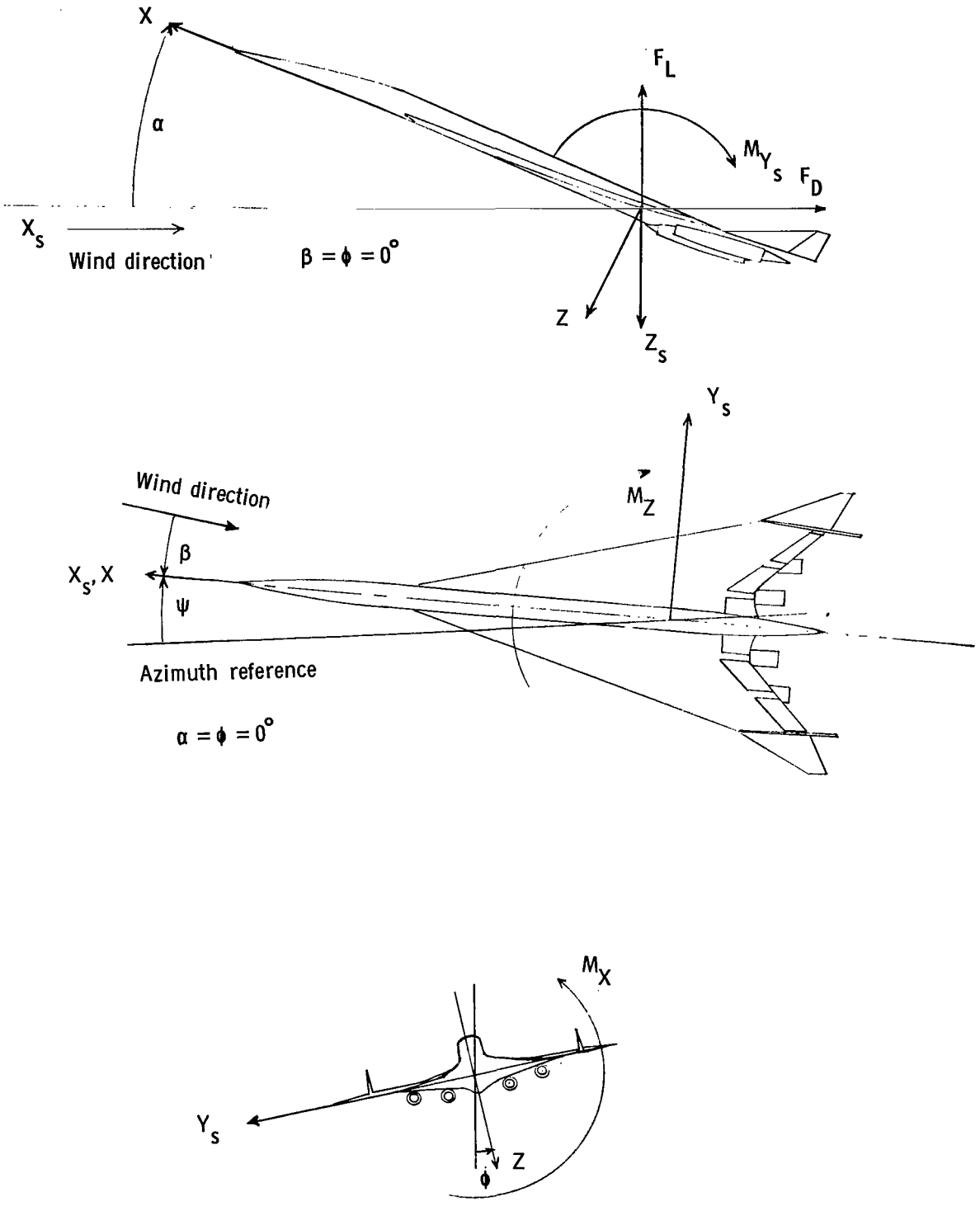

Figure 1.- System of axes used in investigation. Arrows indicate positive directions of moments, forces, and angles.

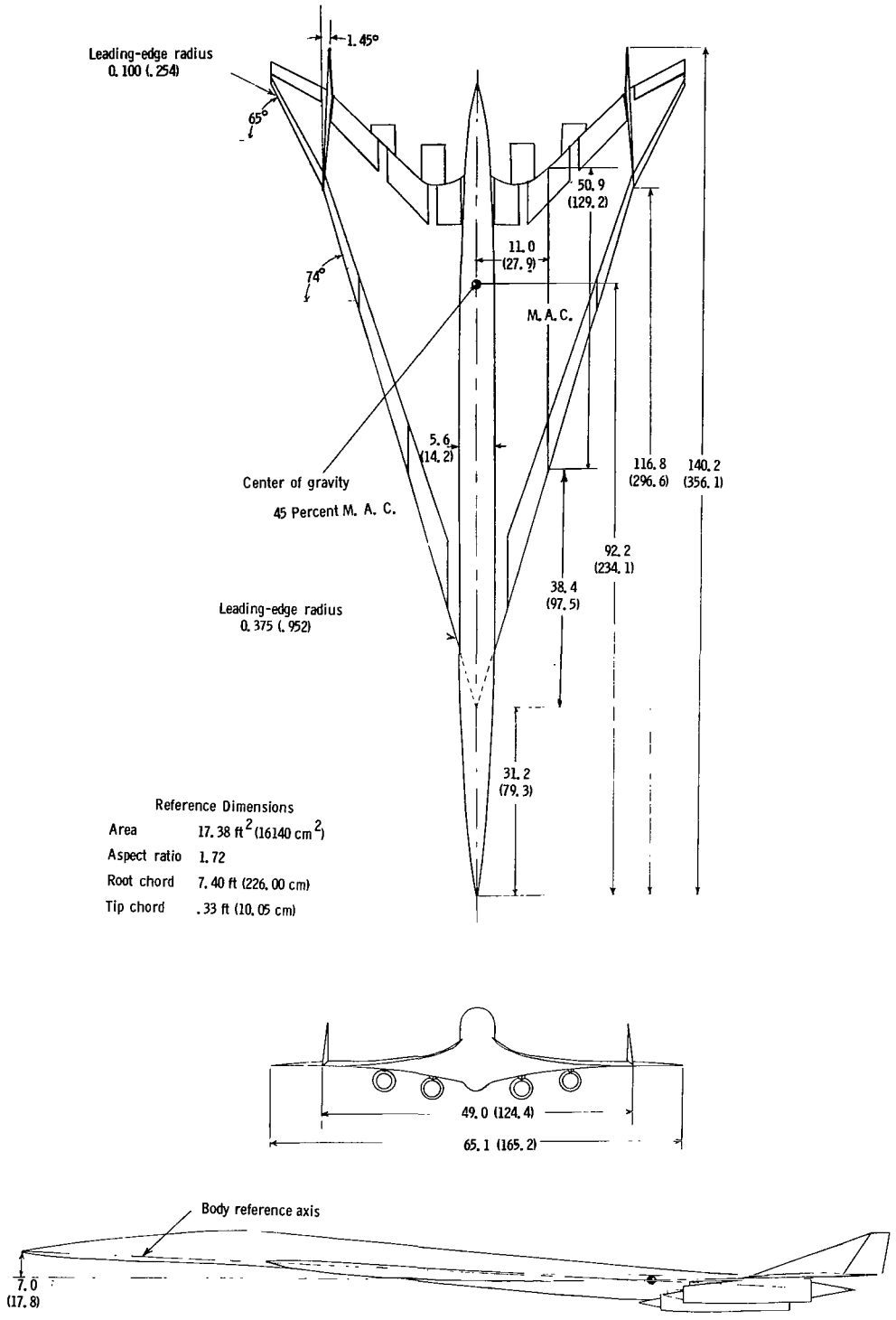

Figure 2.- Three-view drawing of model used in investigation. All dimensions are in inches with centimeters given in parentheses.

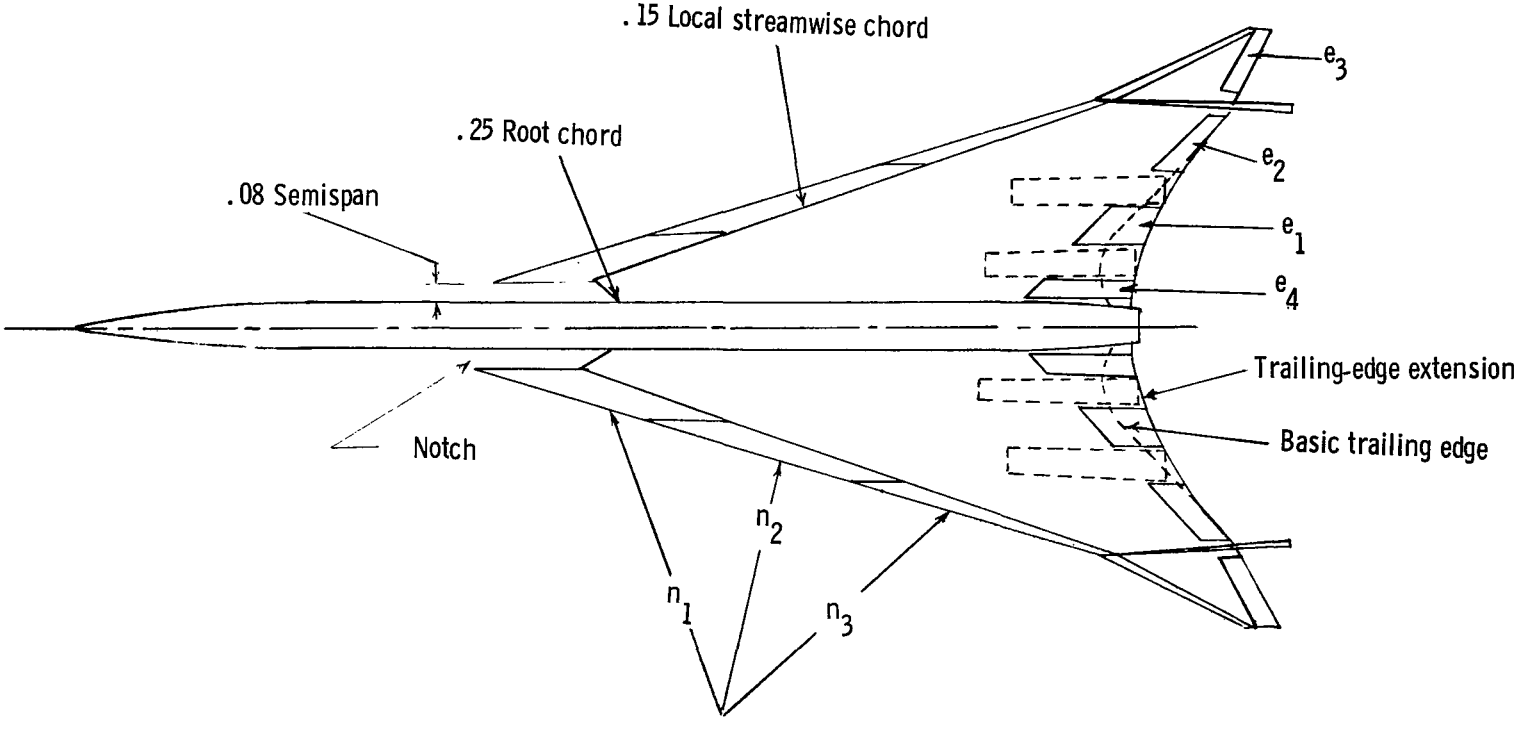

(a) Trailing-edge extension; notch; and leading-edge flaps.

Figure 3.- Modifications to original configuration.

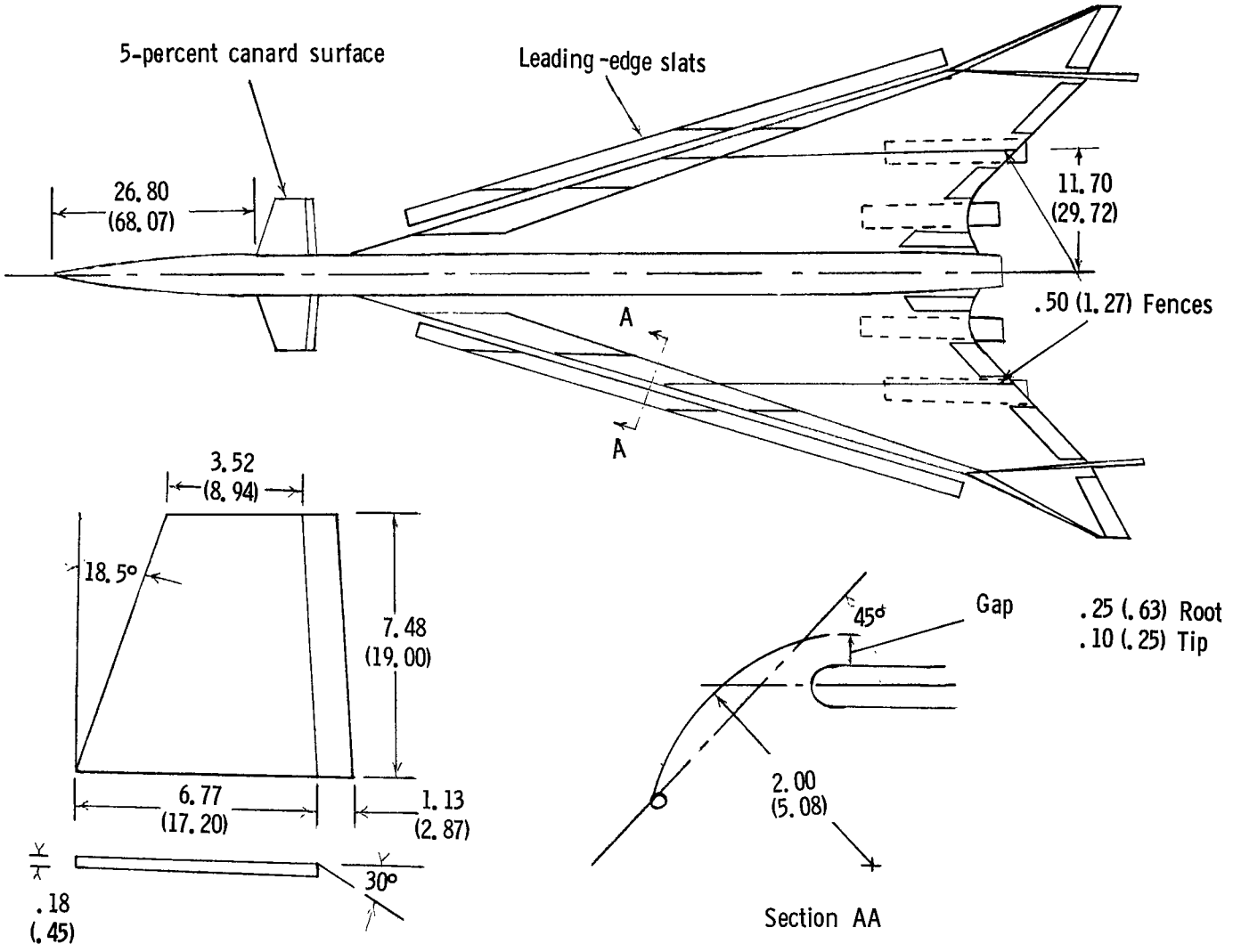

(b) 5-percent canard surface, leading-edge slats, and fences. All dimensions are in inches with centimeters given in parentheses.

Figure 3.- Continued.

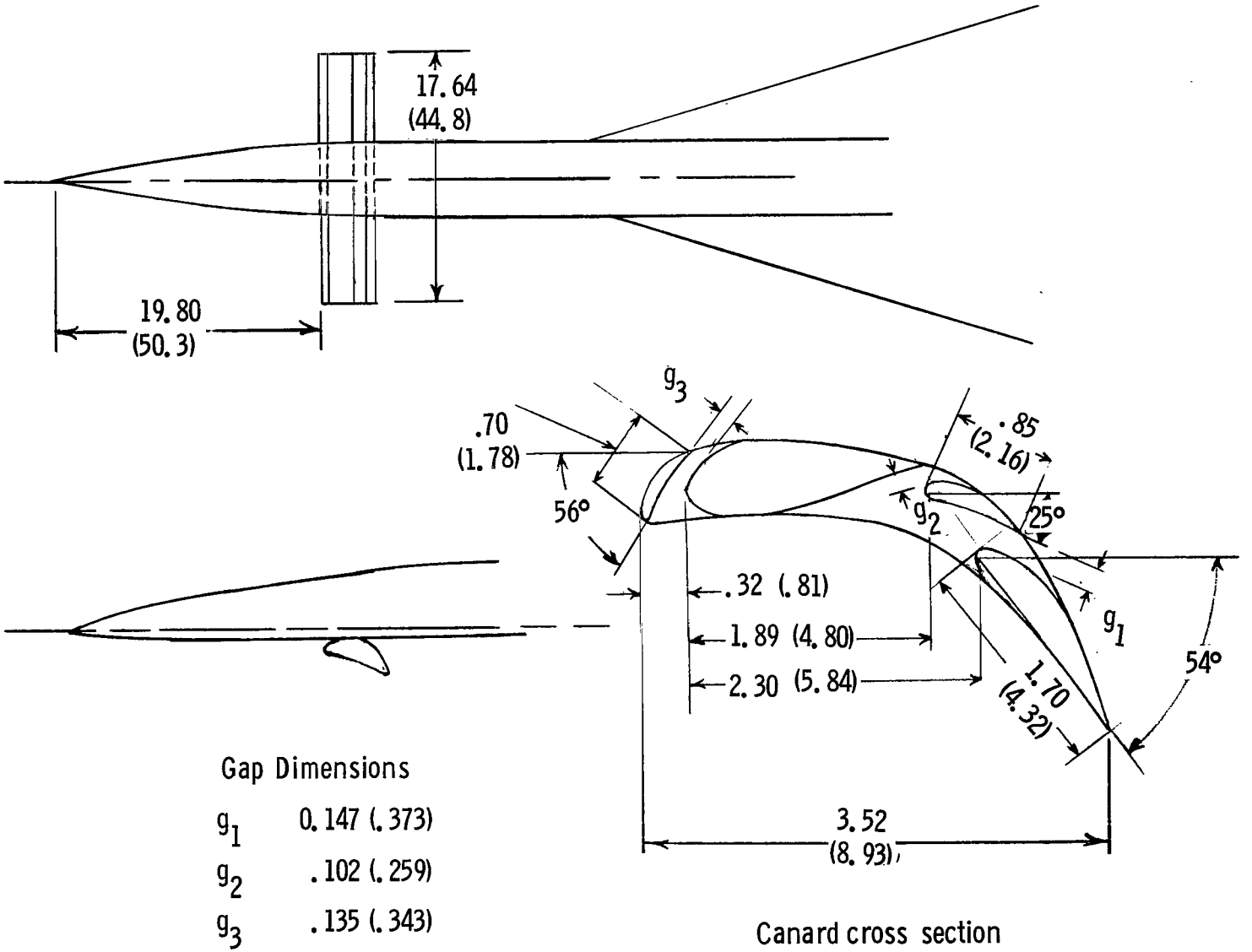

(c) 2-percent canard configuration. All dimensions are in inches with centimeters given in parentheses.

Figure 3.- Concluded.

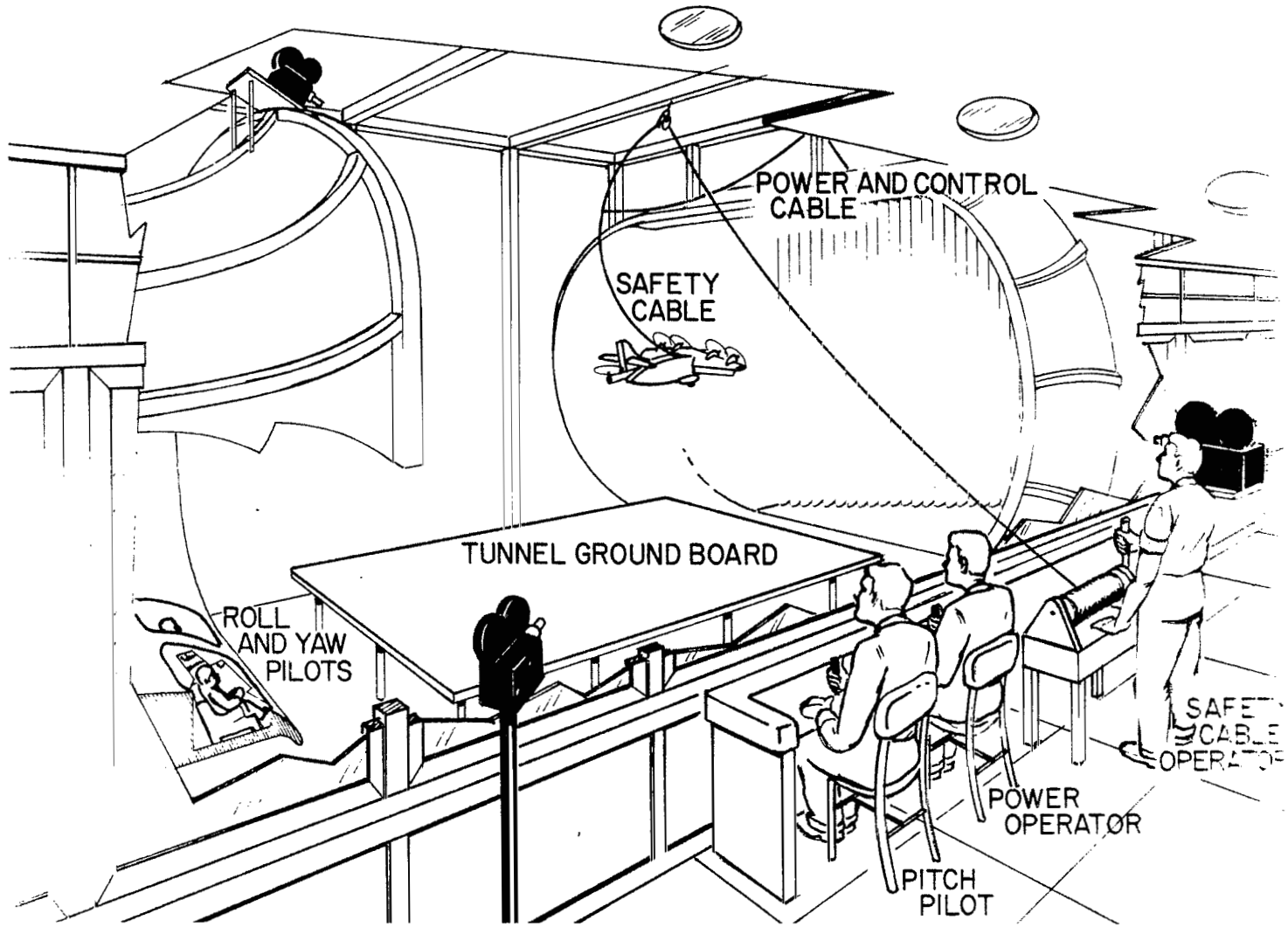

Figure 4.- Setup for flight tests in the Langley full-scale tunnel.

L-64-3008

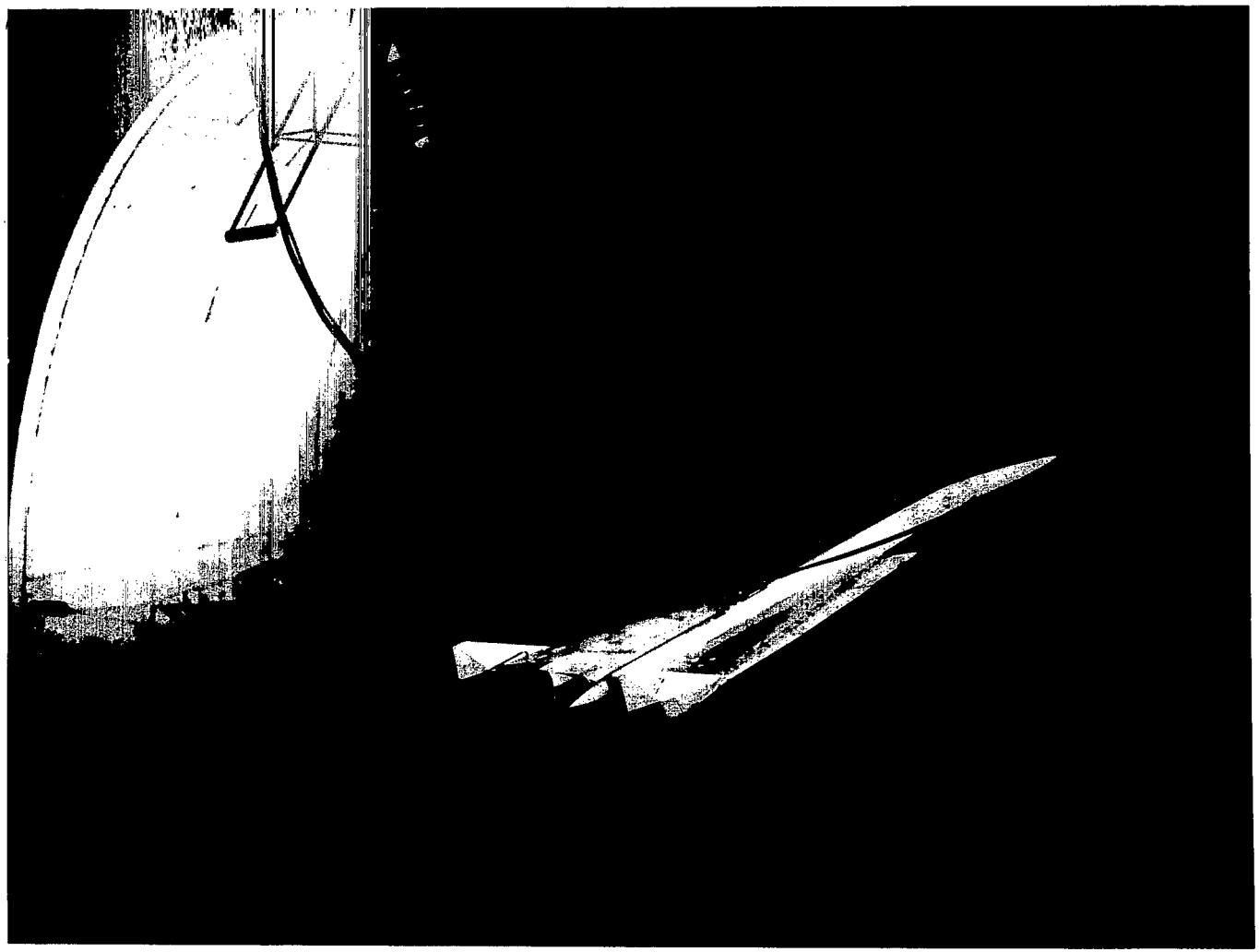

(a) Model flying in the Langley full-scale tunnel. L-65-1763

Figure 5.- Photographs of model.

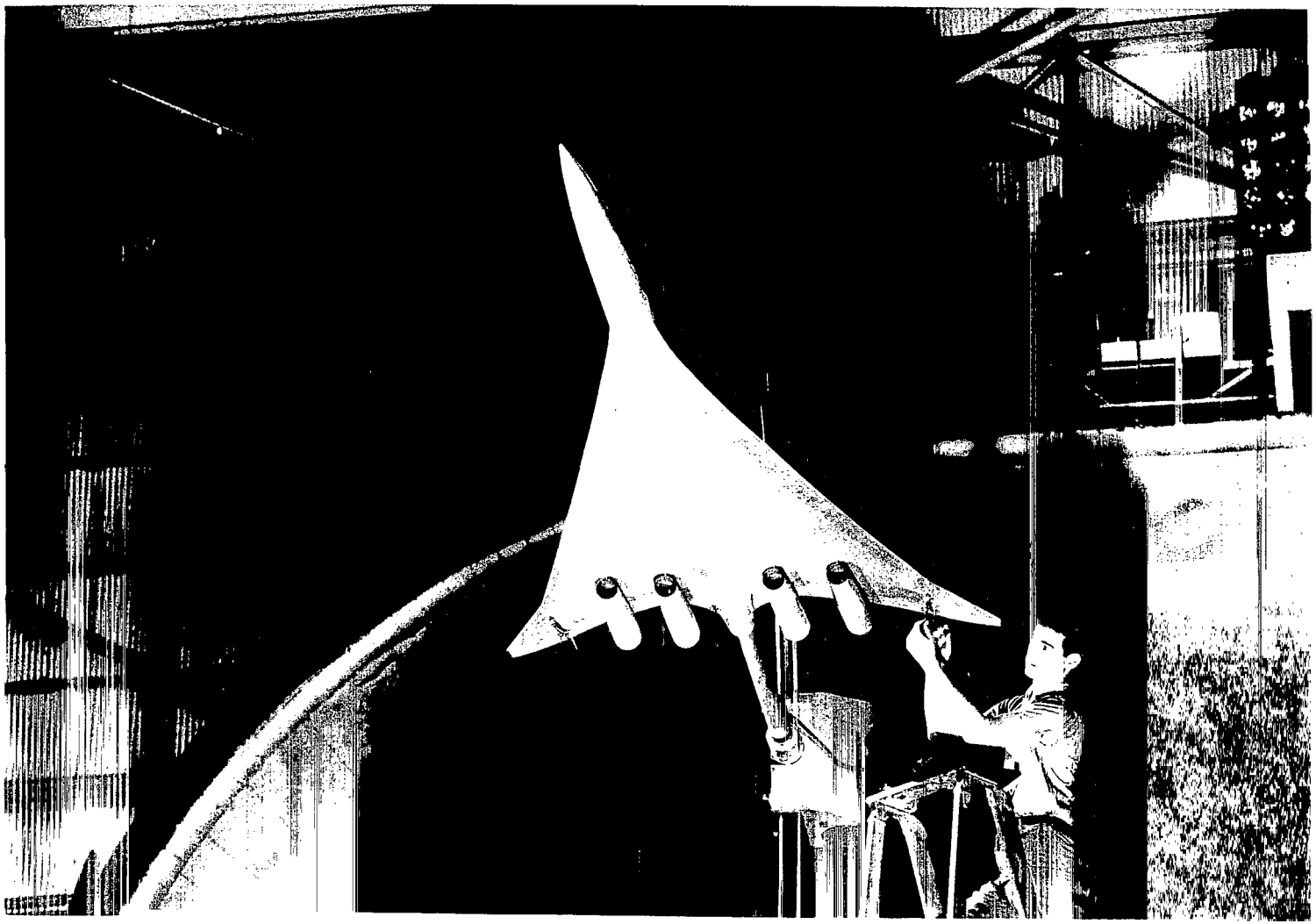

(b) Model mounted on static-force-test equipment in the Langley full-scale tunnel. L-65-1360

Figure 5.- Concluded.

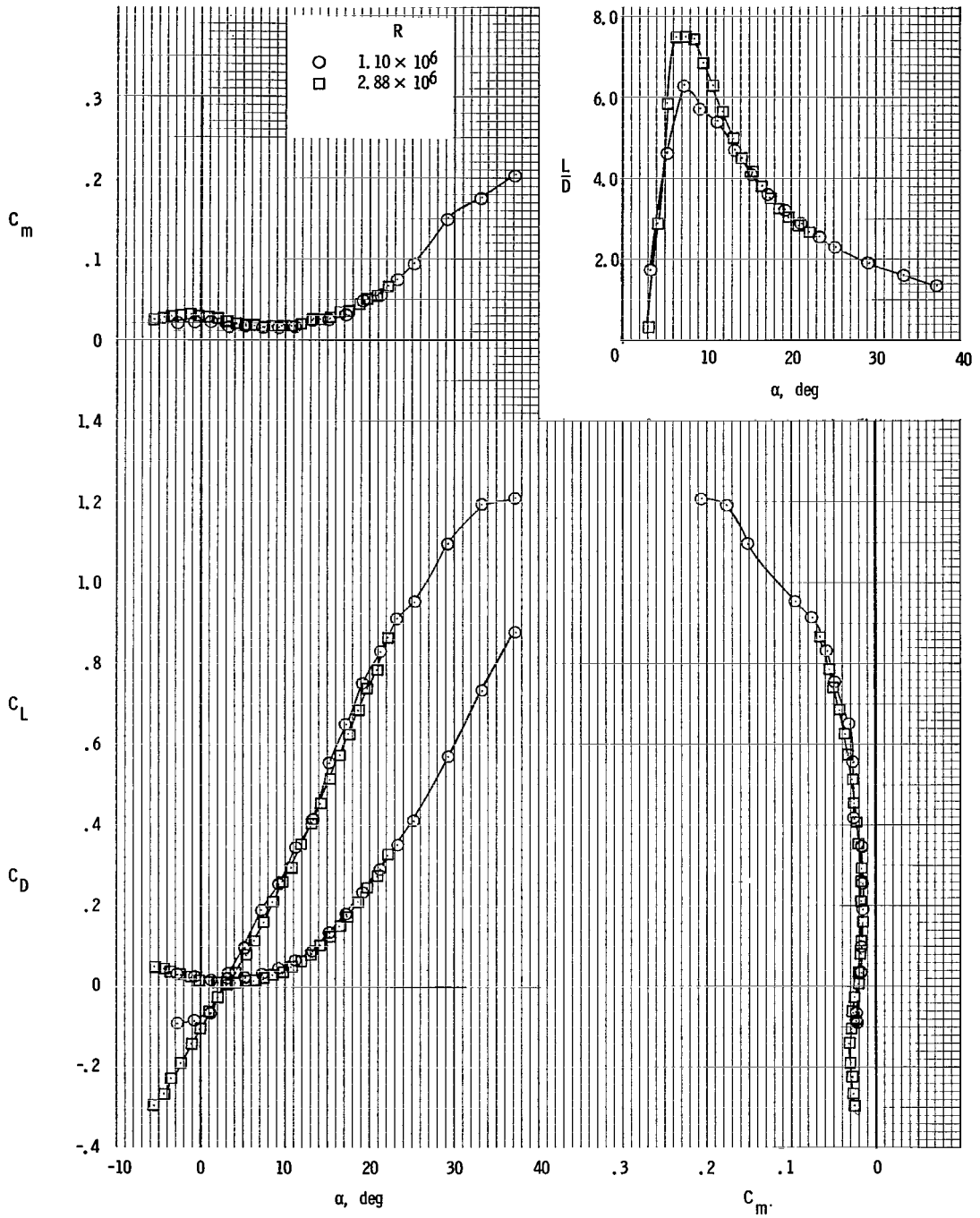

Figure 6.- Comparison of basic longitudinal data with higher Reynolds number data. All controls zero; sharp leading edge; $\delta_{n_1} = \delta_{n_2} = \delta_{n_3} = 0$.

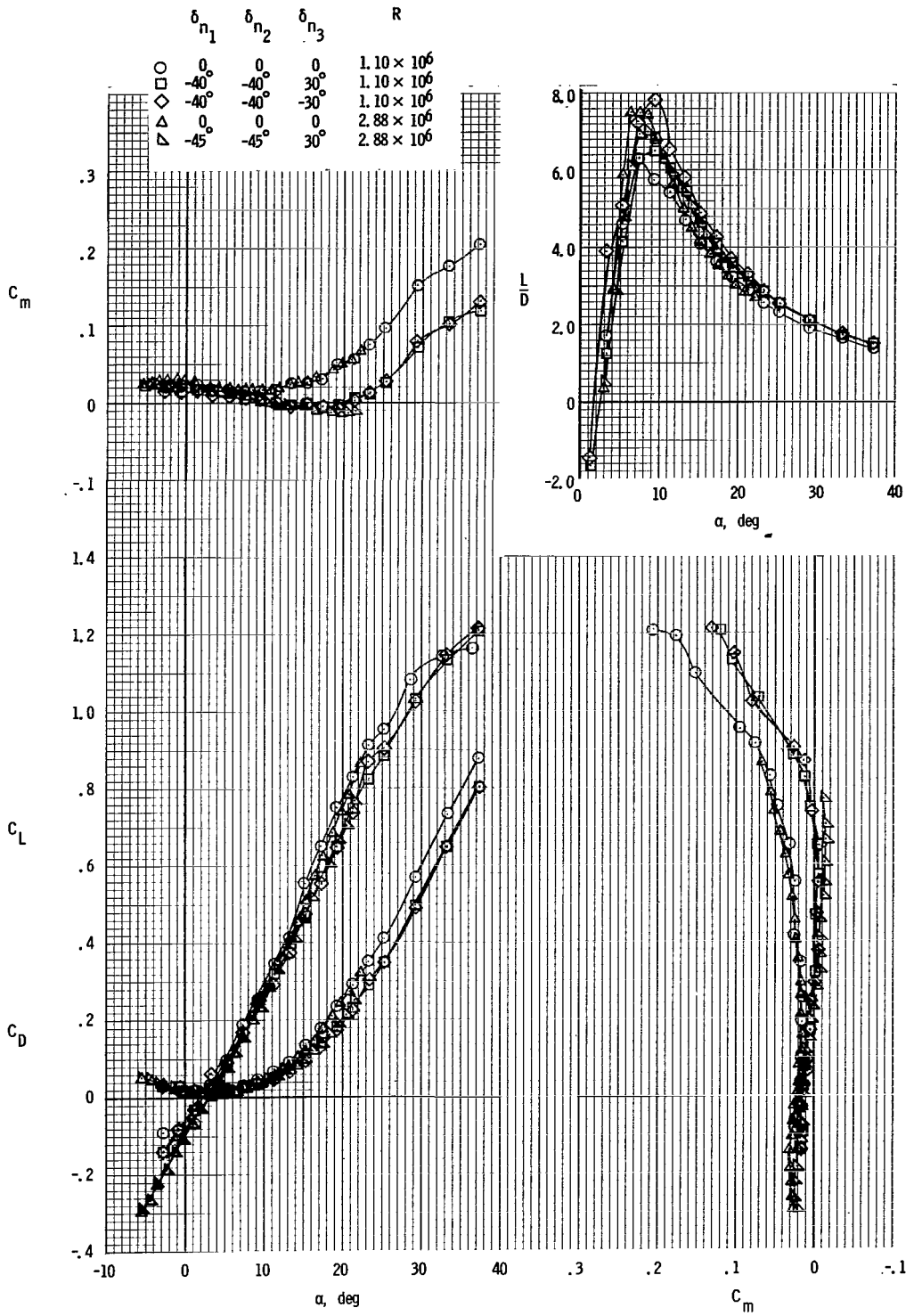

Figure 7.- Effect of leading-edge flap on longitudinal stability characteristics of the model. All controls zero; sharp leading edge.

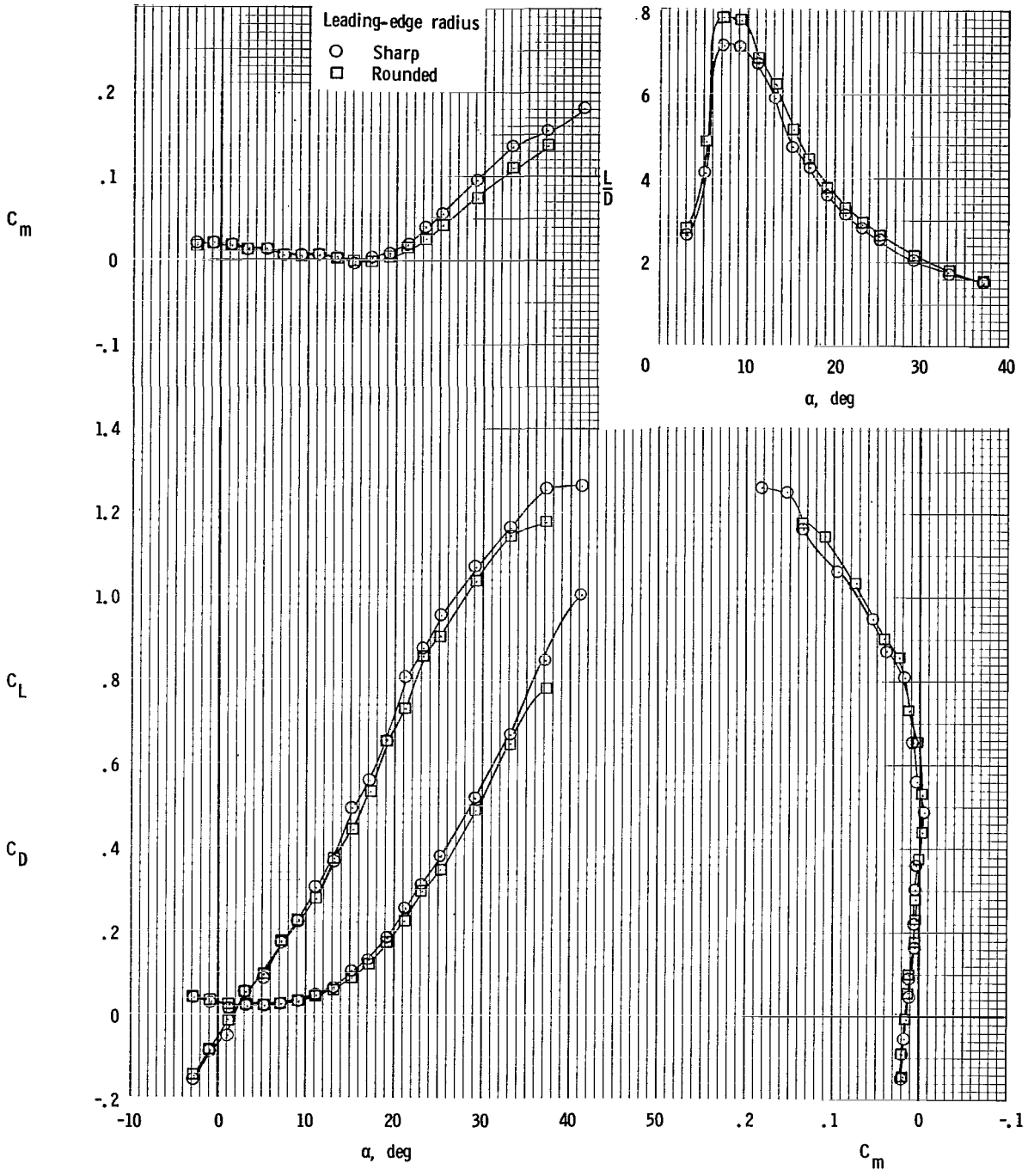

Figure 8.- Effect of leading-edge radius on longitudinal stability characteristics of model. $\delta_{n_1} = \delta_{n_2} = \delta_{n_3} = -30^0$.

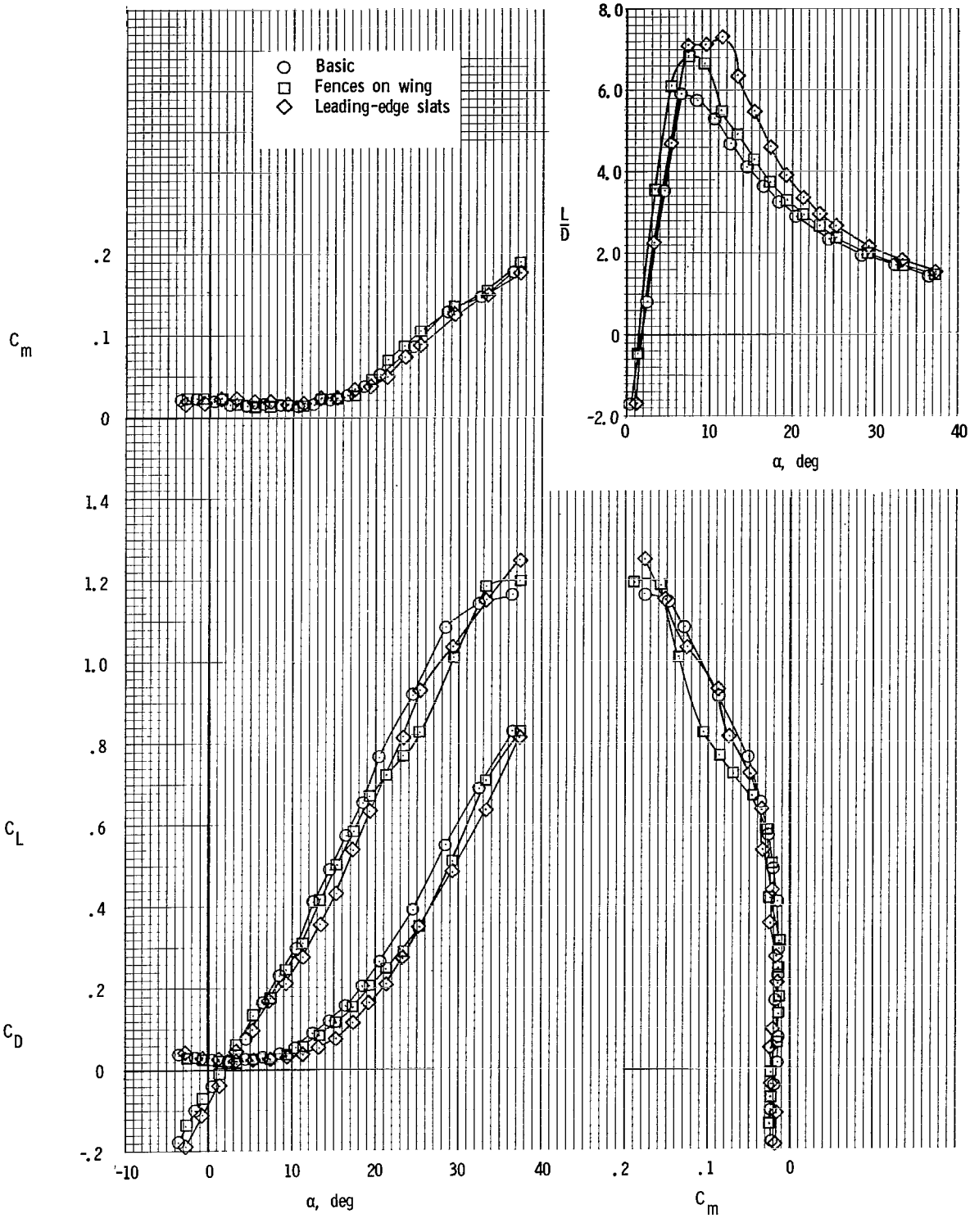

Figure 9.- Effect of fences and leading-edge slats on longitudinal stability characteristics of model. All controls zero; $\delta_{n_1} = \delta_{n_2} = \delta_{n_3} = 0$.

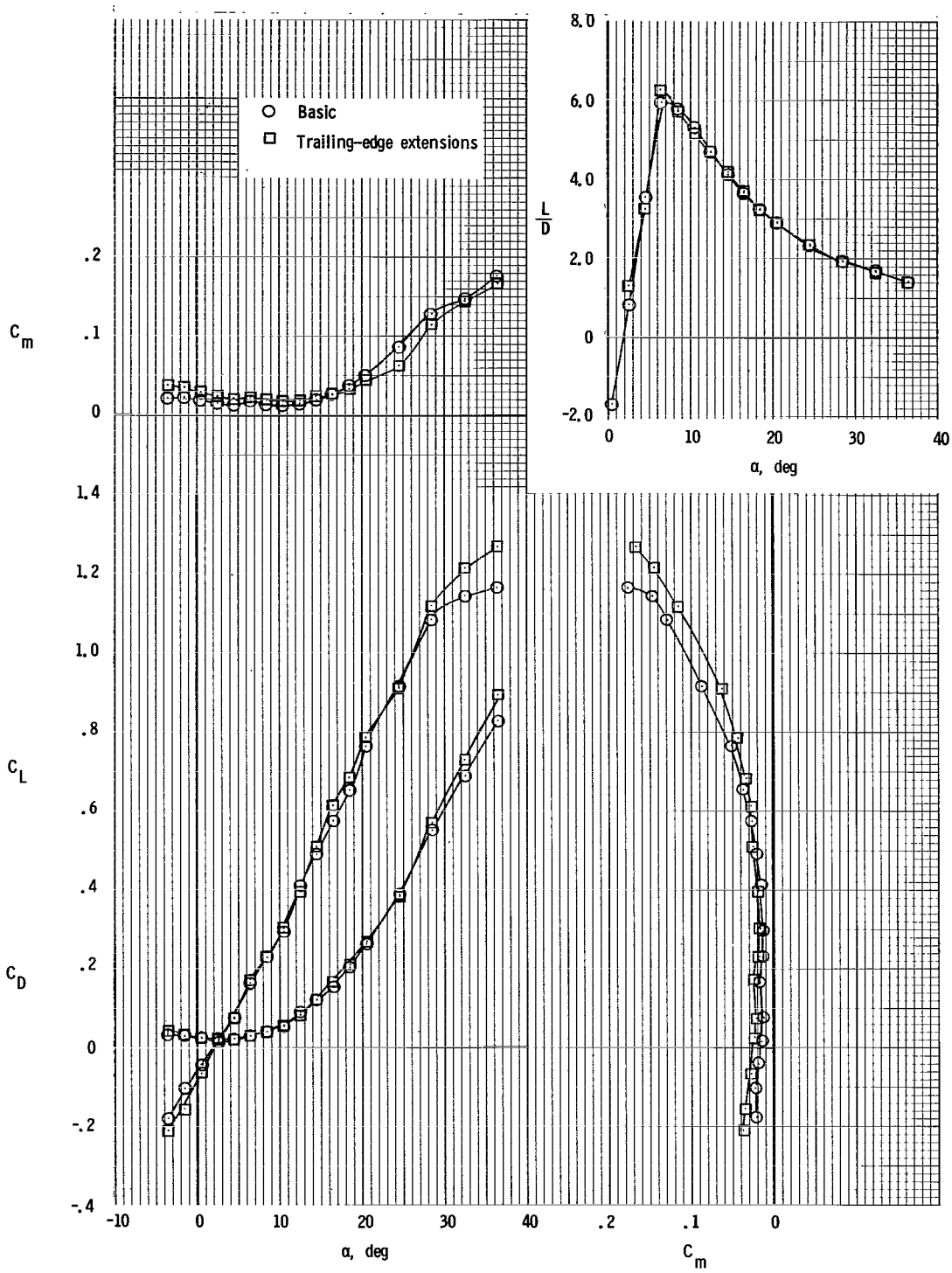

Figure 10.- Effect of trailing-edge extension on static longitudinal stability characteristics of model. All controls zero.

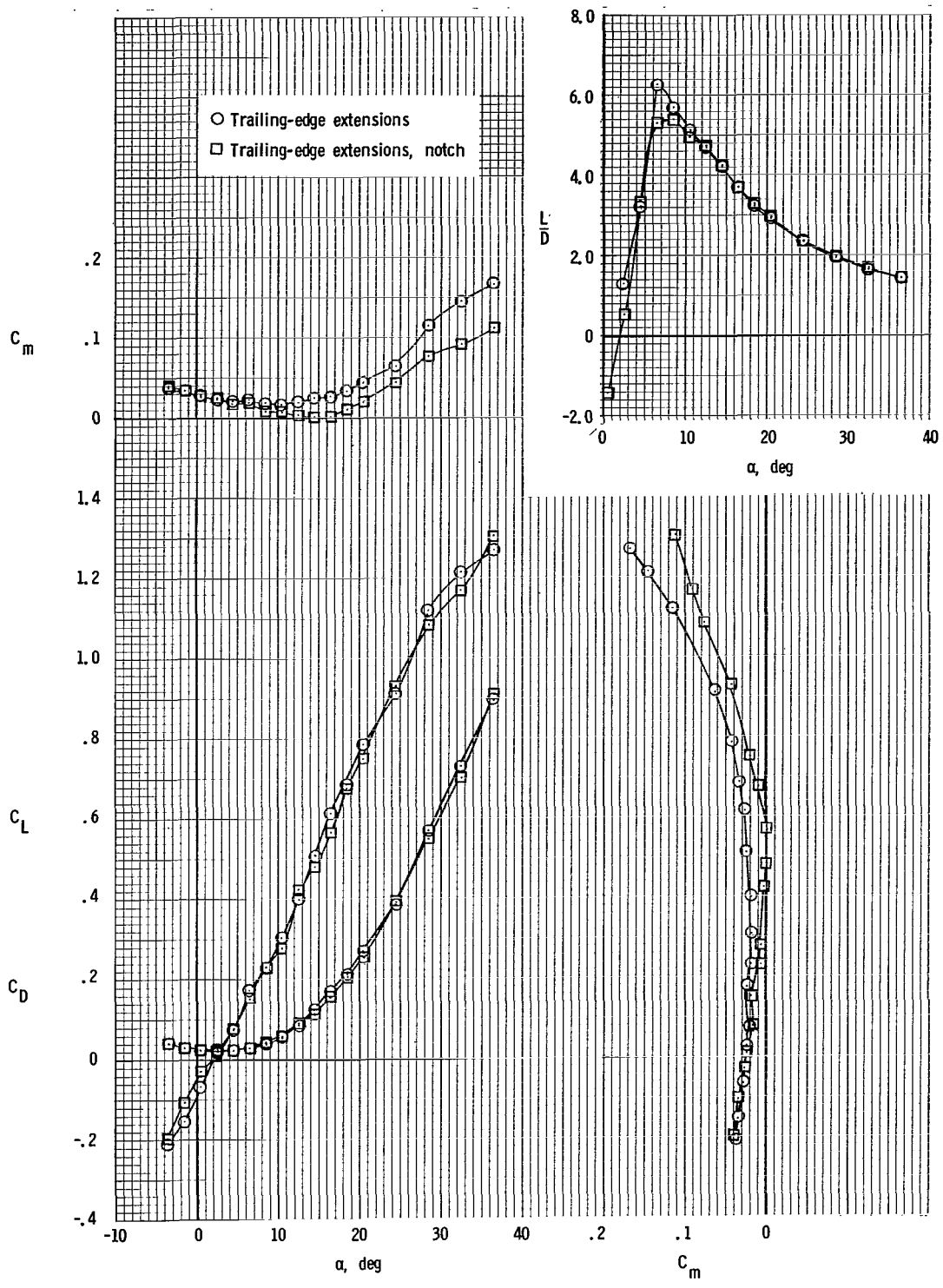

Figure 11.- Effect of wing apex notch on static longitudinal stability characteristics of model. All controls zero.

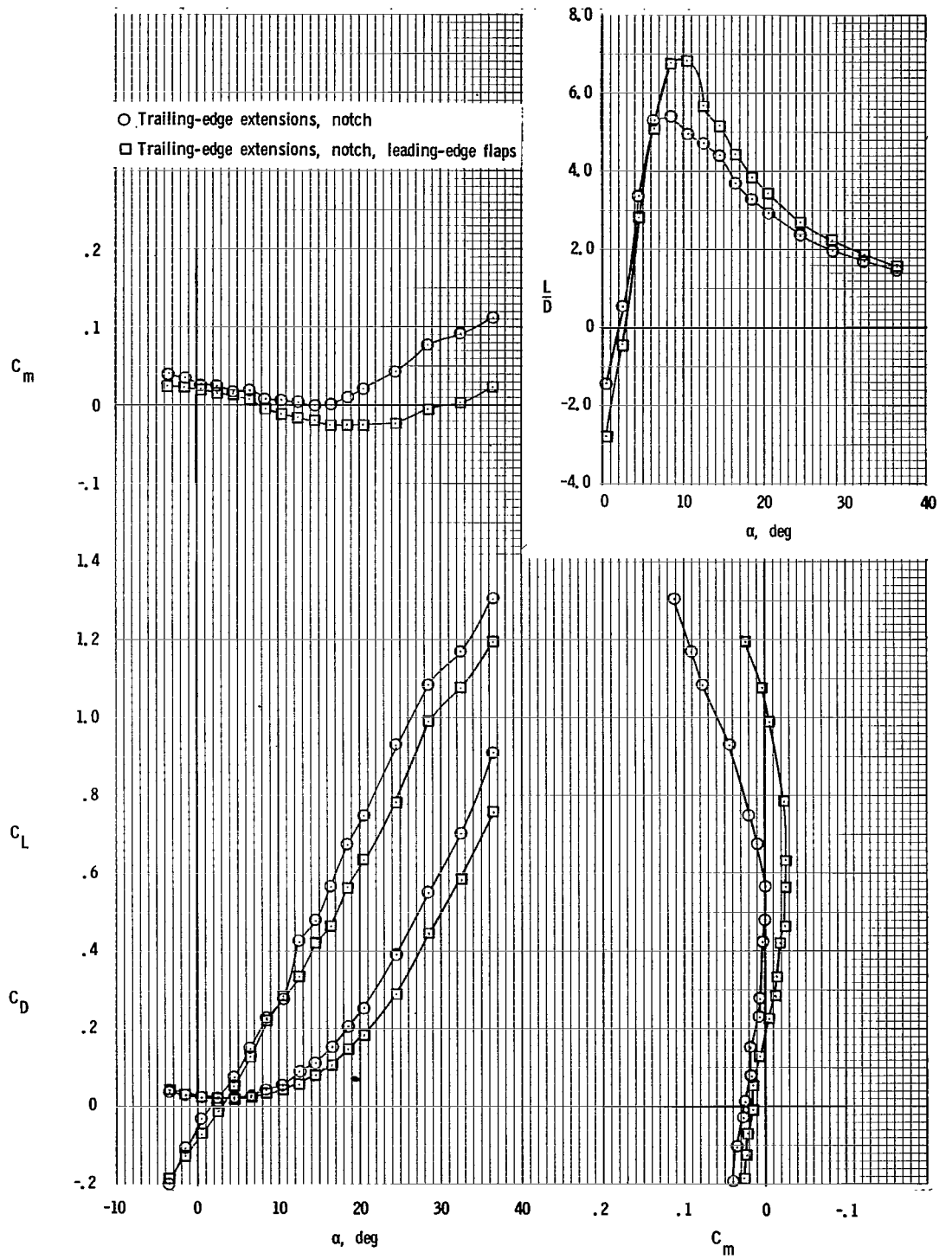

Figure 12.- Effect of leading-edge flaps in conjunction with trailing-edge extension and notch. All controls zero.

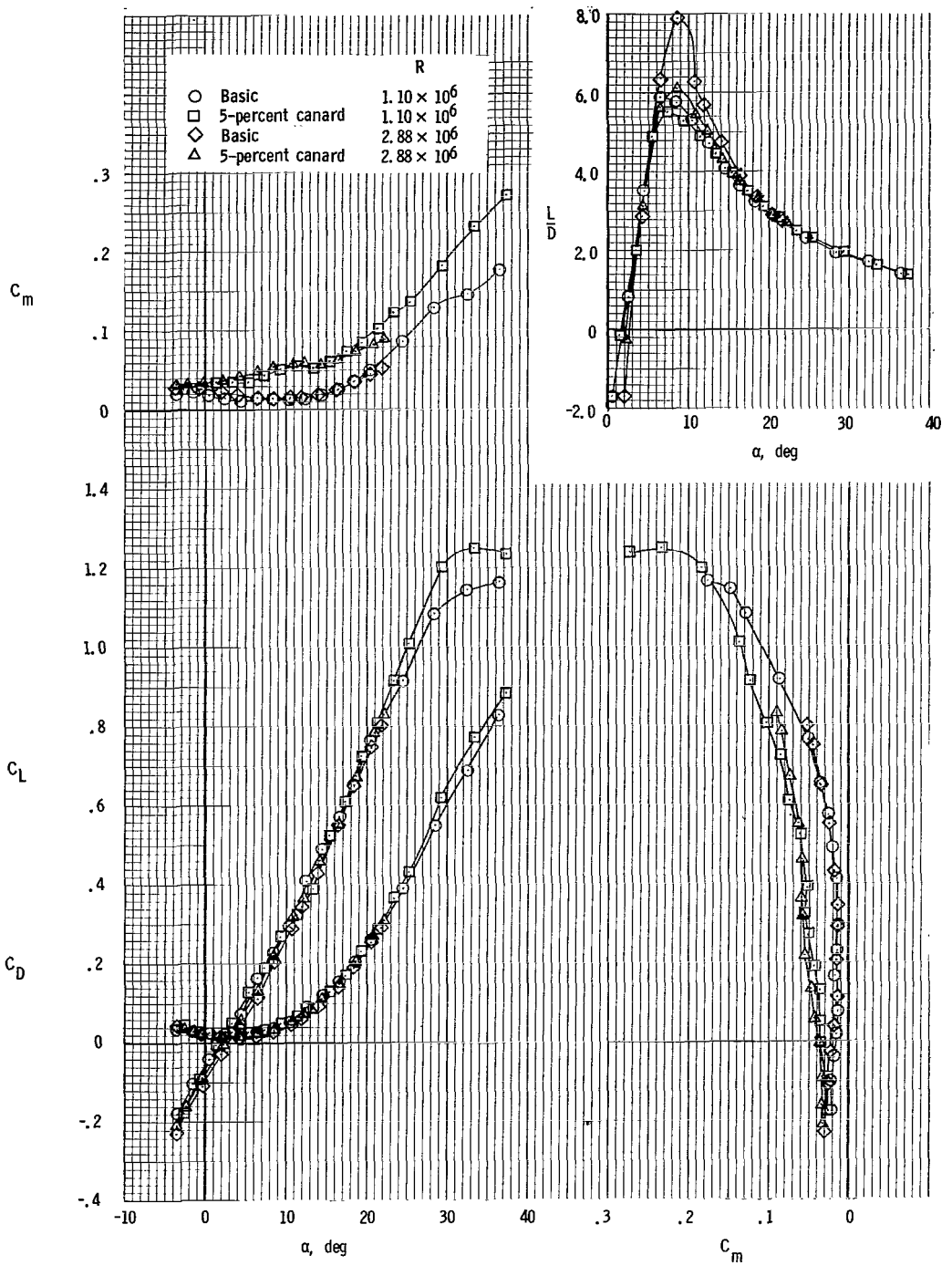

Figure 13.- Effect of a 5-percent canard on longitudinal stability characteristics of model. All controls zero; $\delta_{n_1} = \delta_{n_2} = \delta_{n_3} = 0$.

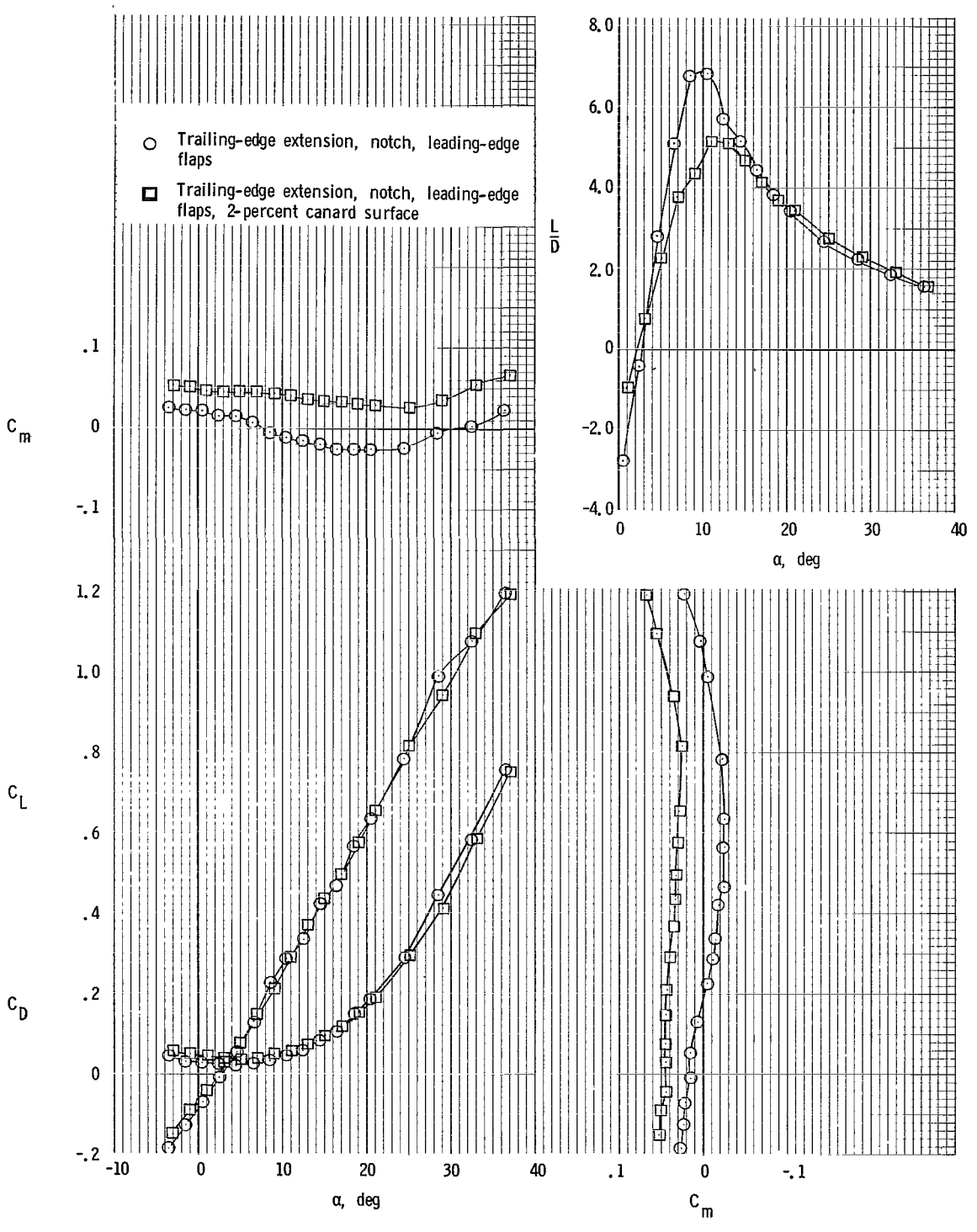

Figure 14.- Effect of high lift canard in conjunction with trailing-edge extension, wing apex notch, and leading-edge flaps. All controls zero.

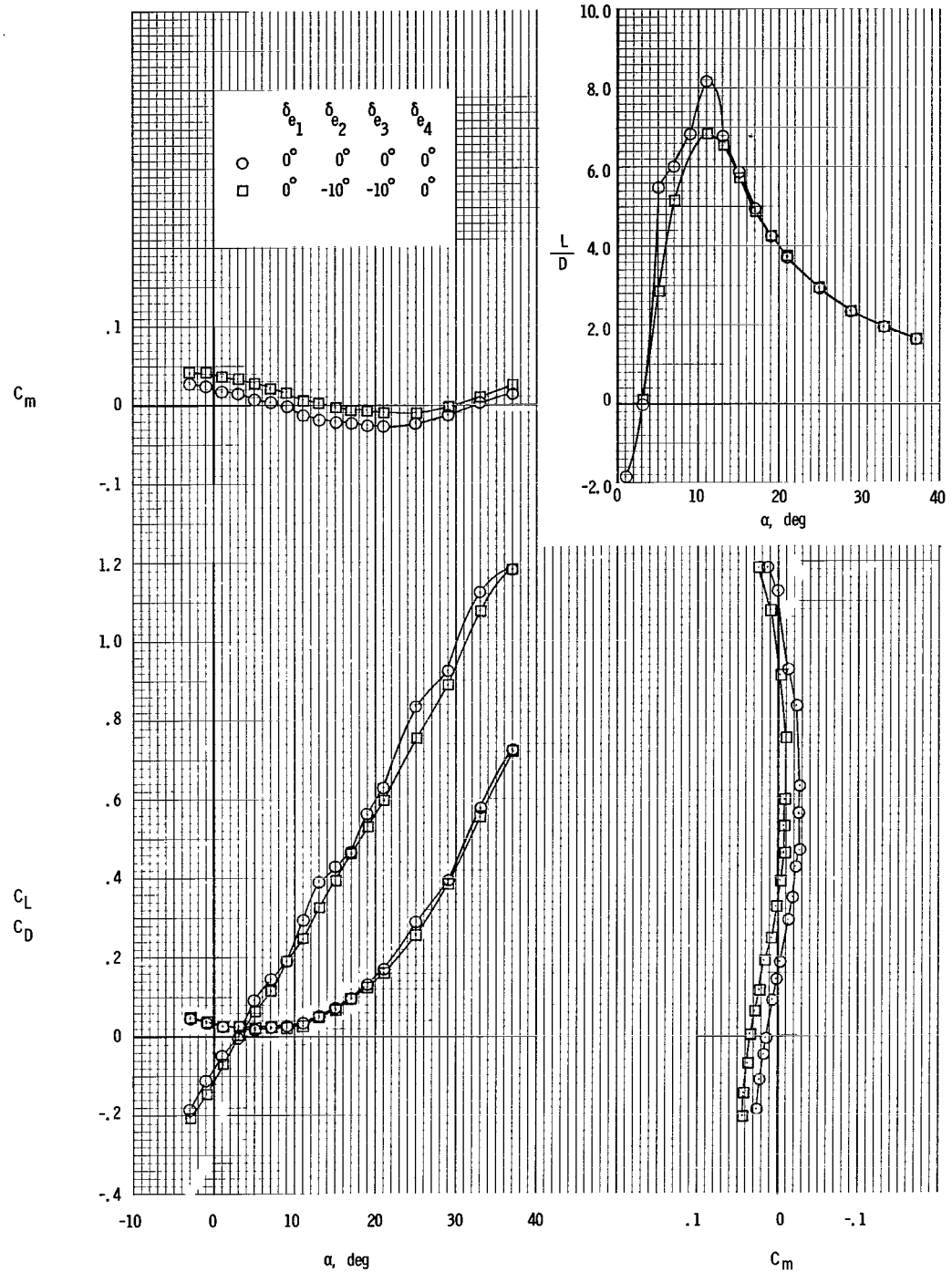

(a) Canard off.

Figure 15.- Longitudinal control characteristics of model. Trailing-edge extension; notch; and leading-edge flaps.

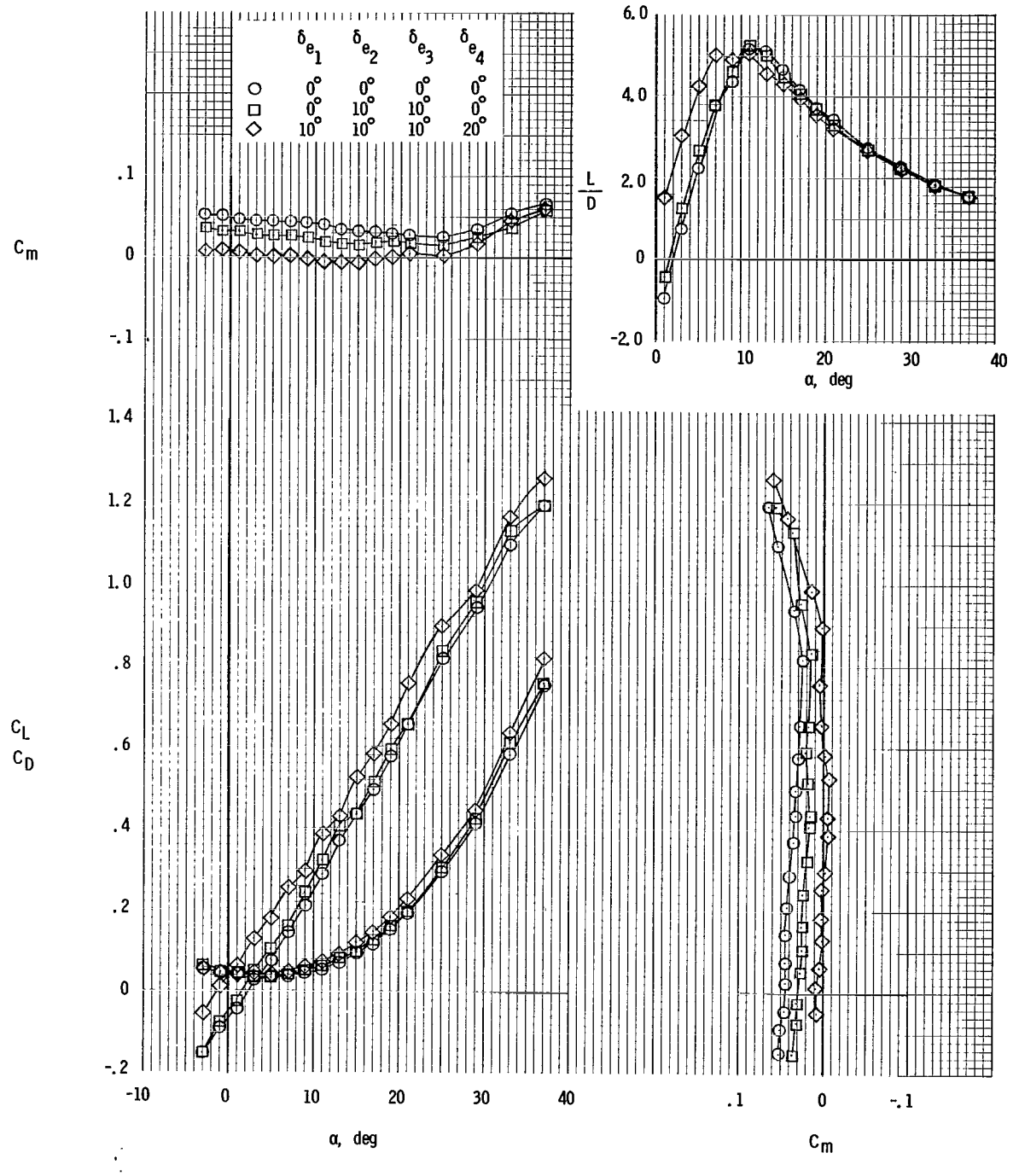

(b) 2-percent canard on.

Figure 15.- Concluded.

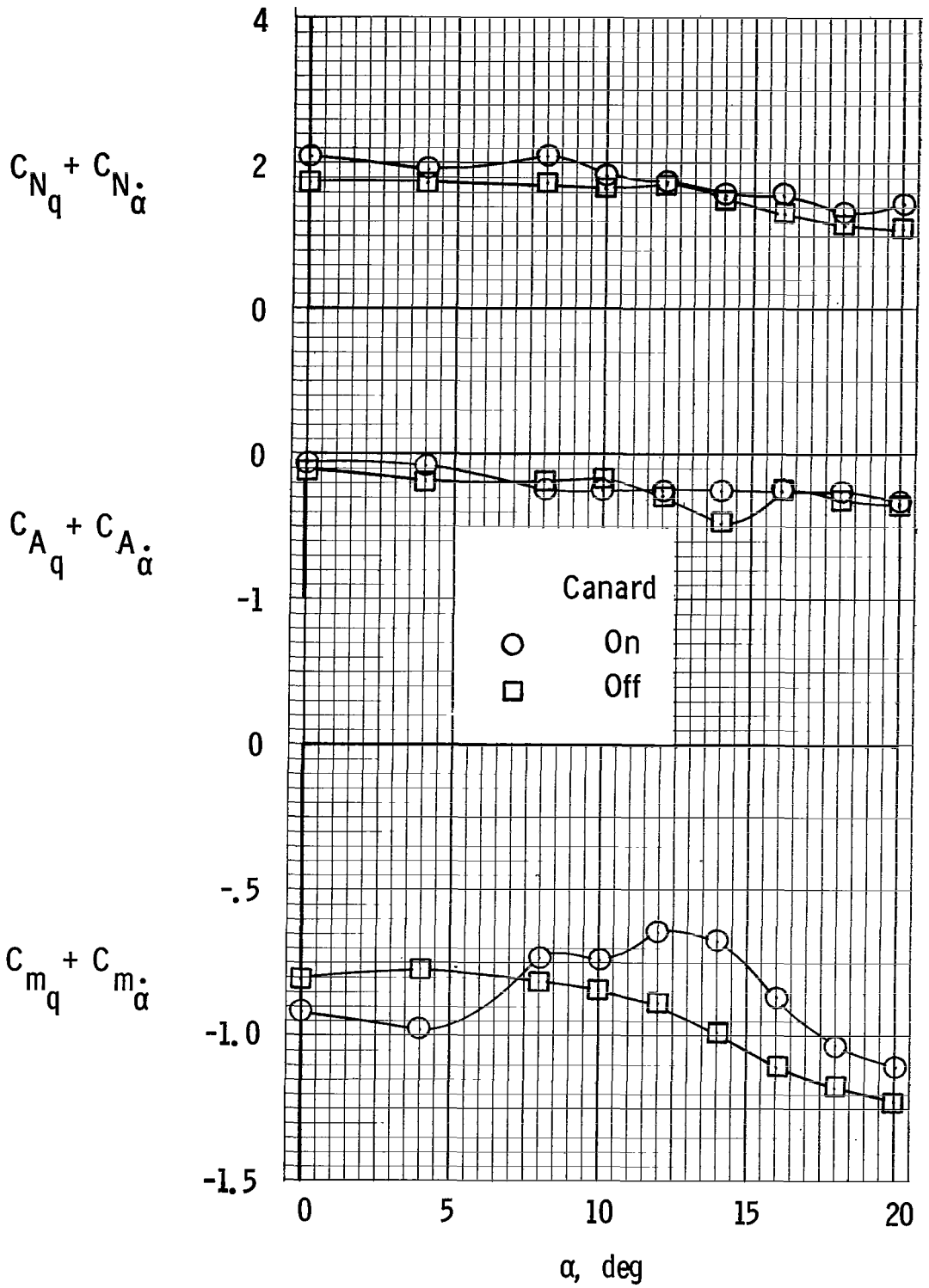

Figure 16.- Pitching oscillation derivatives. All controls zero; k = 0.091; trailing-edge extension; notch; and leading-edge flaps.

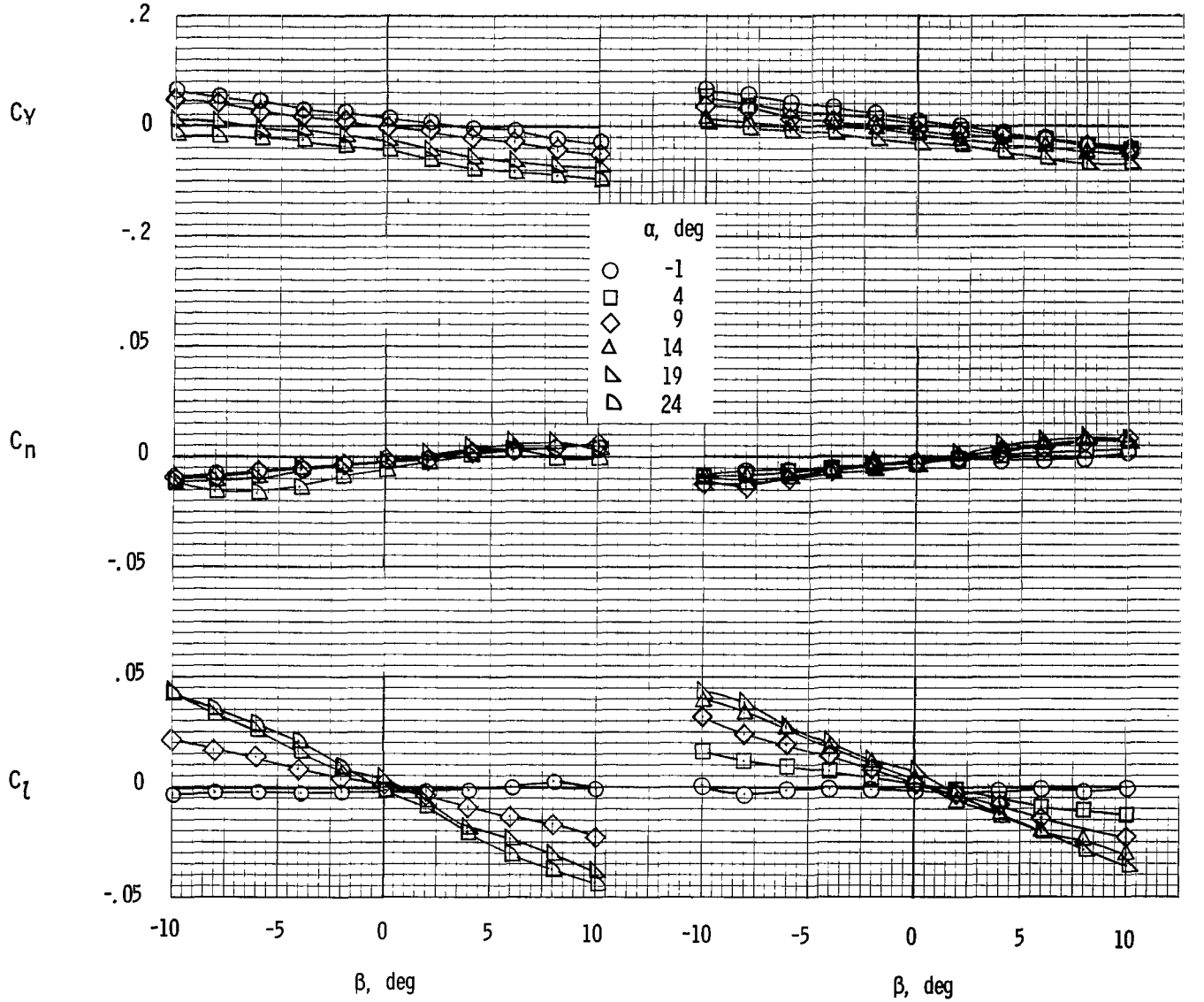

(a) Canard off.

(b) 2-percent canard on.

Figure 17.- Static-lateral-stability parameters of model. Trailing-edge extension; notch; and leading-edge flaps.

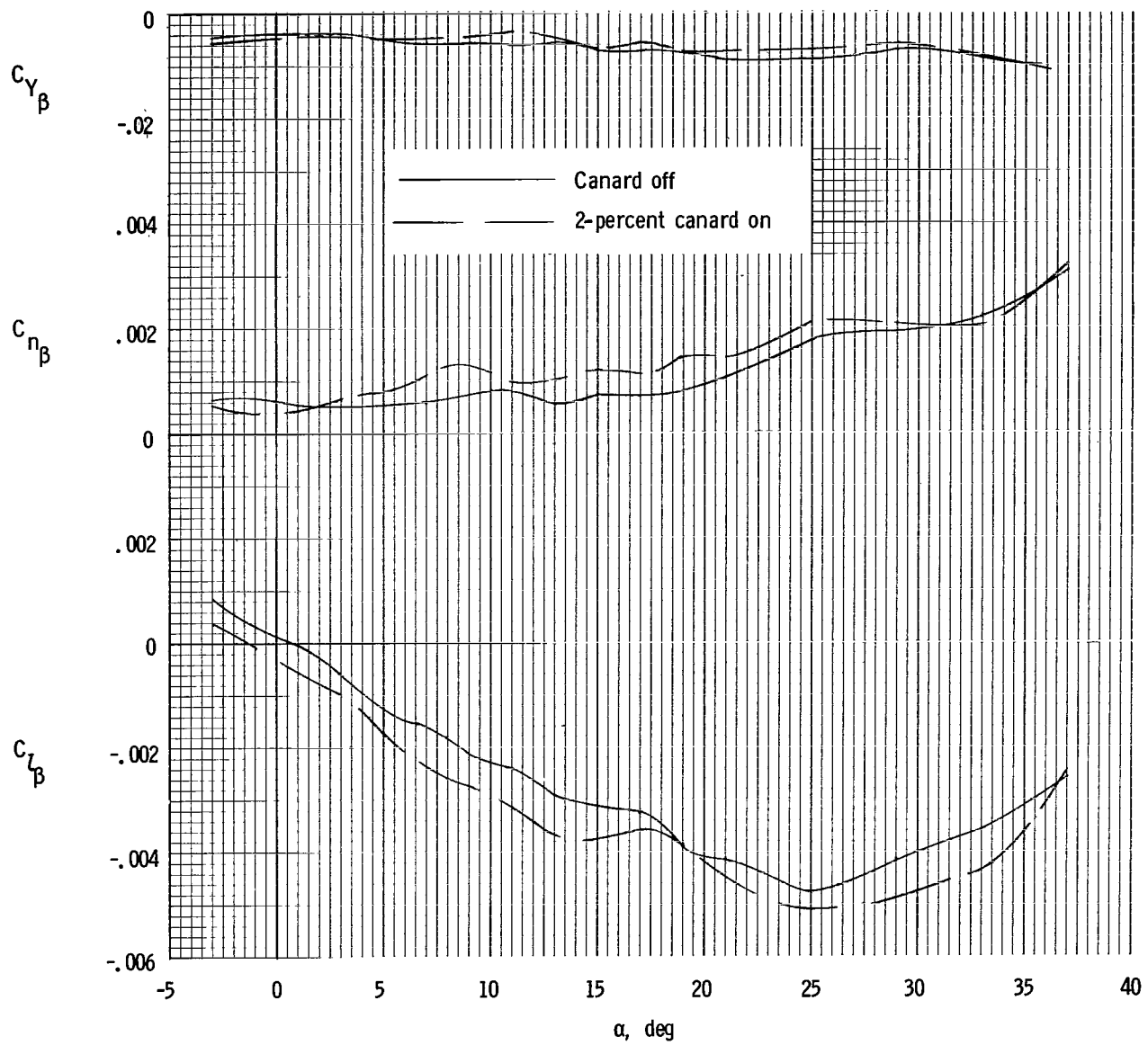

Figure 18.- Static-lateral-stability parameters of model.

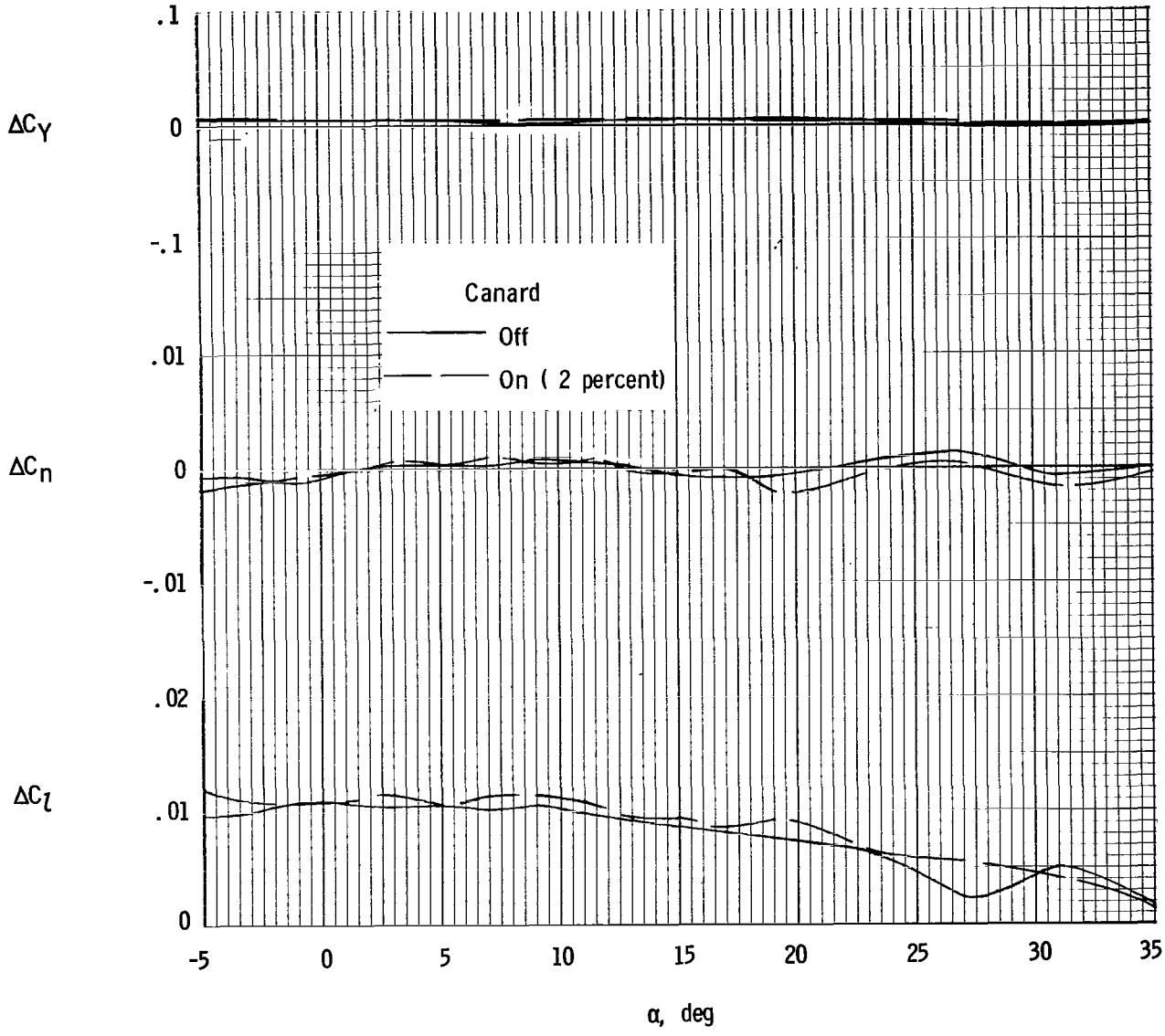

Figure 19.- Total aileron effectiveness of model configurations tested in flight. $\delta_a = 22^0$ on surfaces e_2 and e_3; trailing-edge extension; notch; and leading-edge flaps.

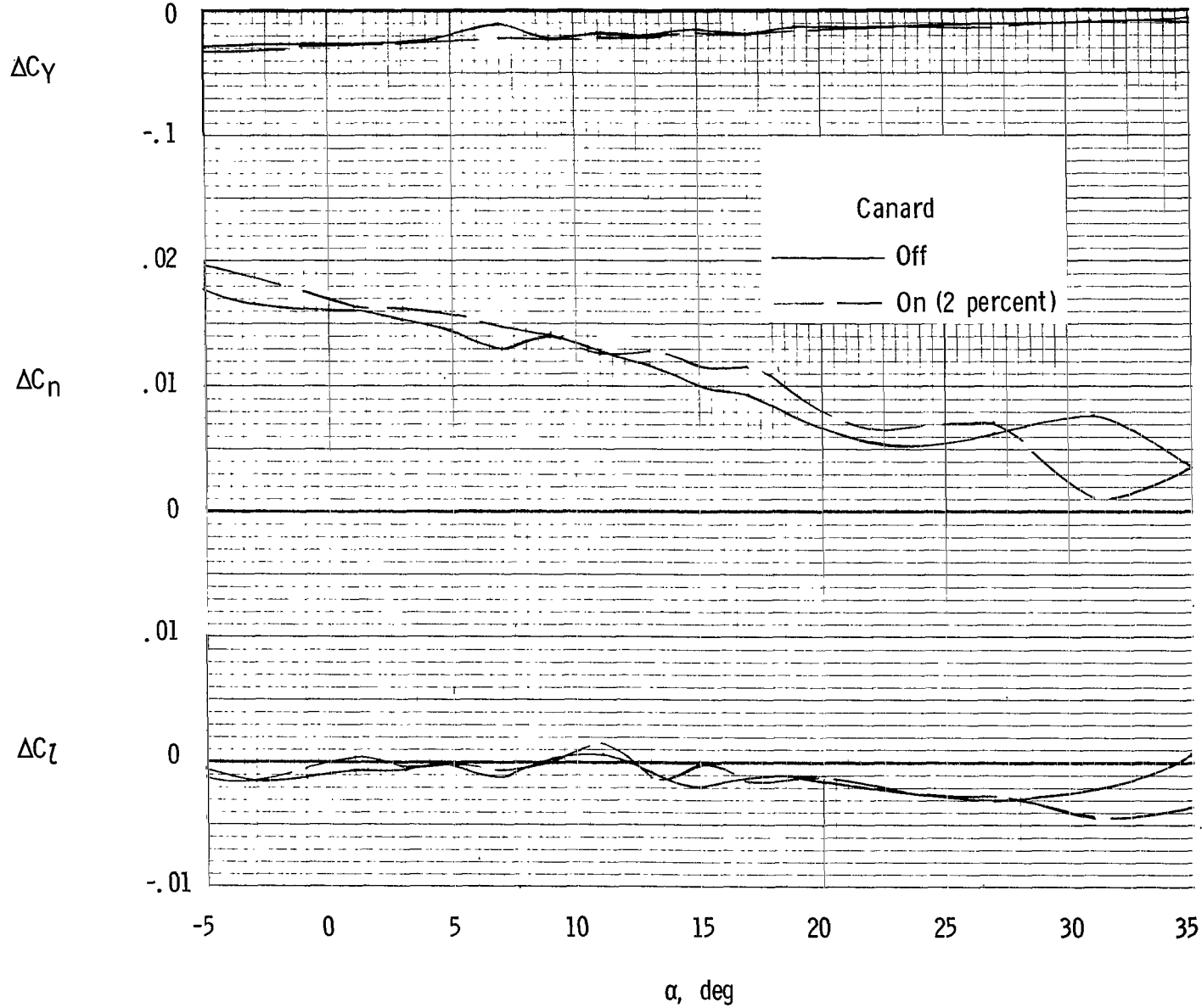

Figure 20.- Rudder effectiveness of the model configurations that were tested in flight. $\delta_r = 20^o$; trailing-edge extension; notch; and leading-edge flaps.

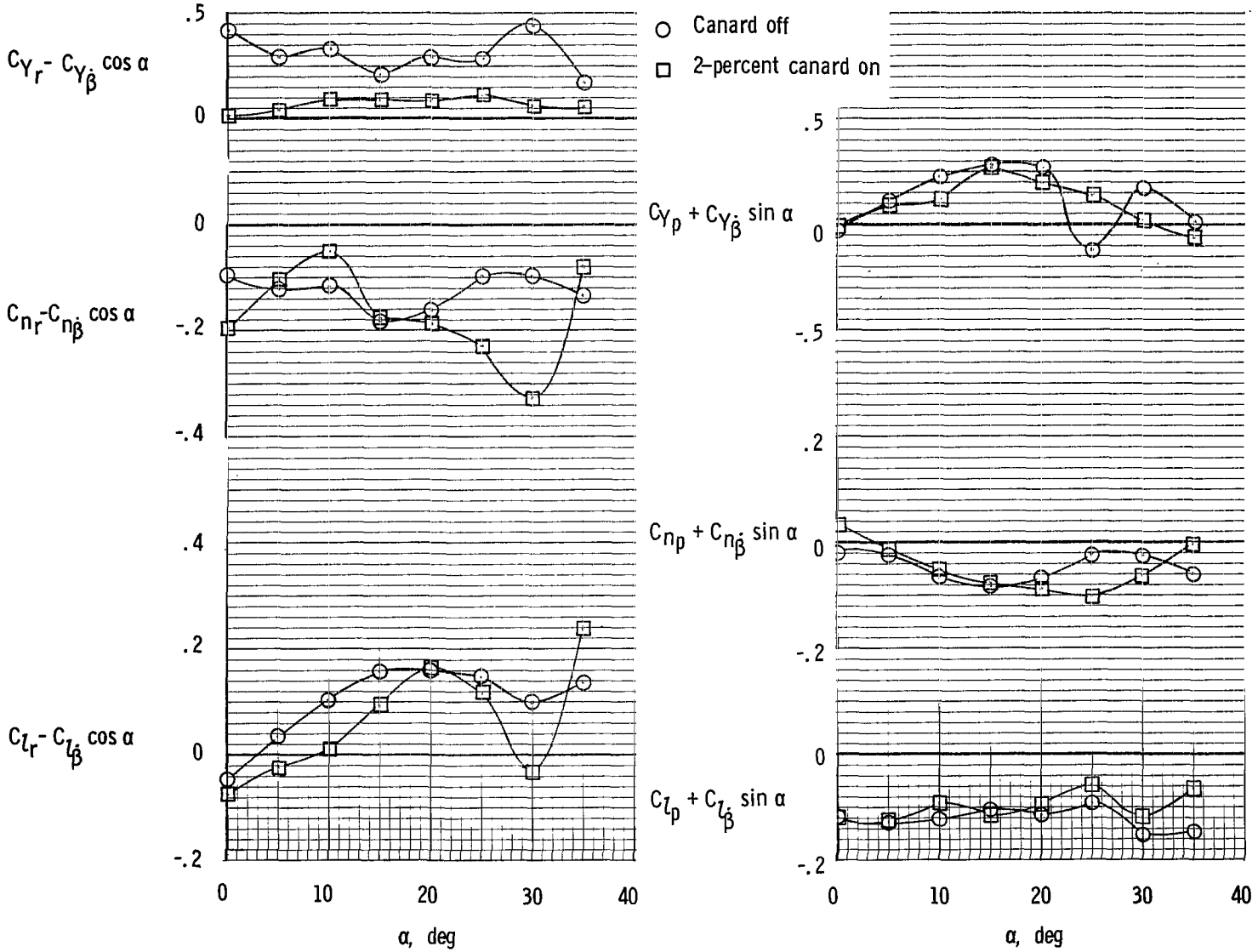

(a) Yawing derivatives.

(b) Rolling derivatives.

Figure 21.- Lateral oscillatory derivatives of model configurations tested in flight. Trailing-edge extension; notch; and leading-edge flaps.

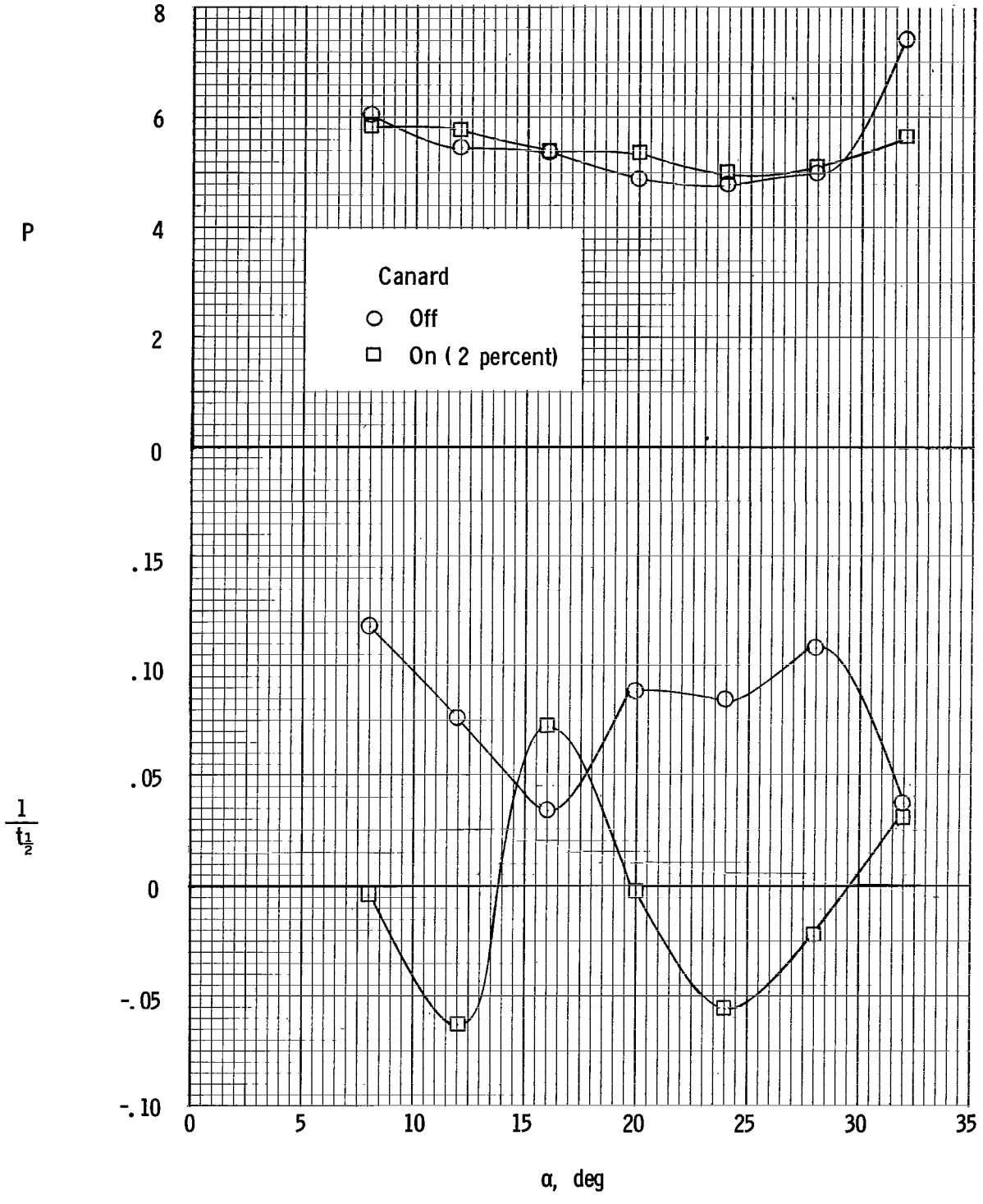

Figure 22.- Calculated period and damping characteristics of Dutch roll oscillation for the full-scale configuration. Calculations based on measured force-test data of present investigation. Trailing-edge extension; notch; and leading-edge flaps.

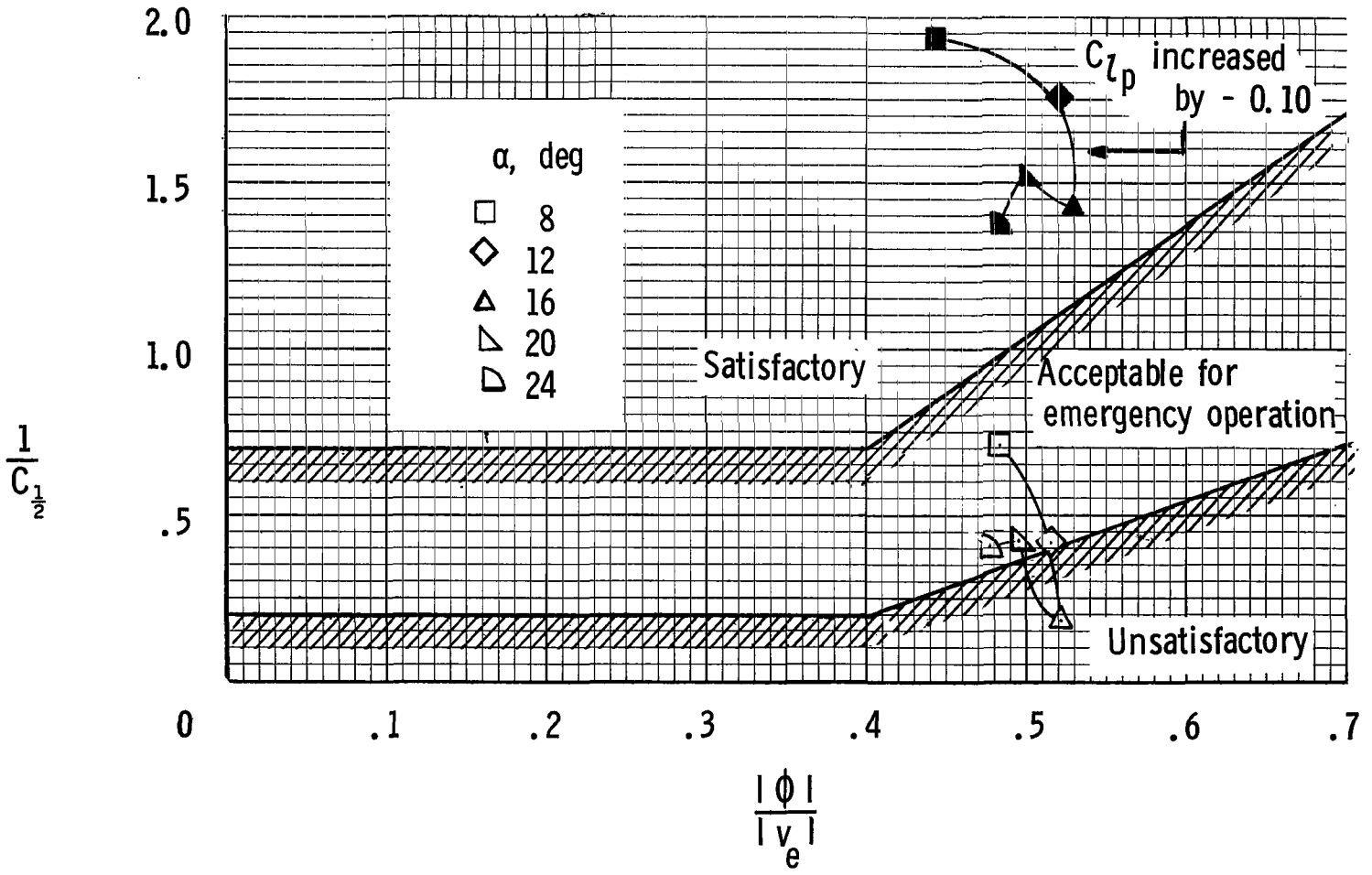

(a) Canard off.

Figure 23.- Lateral oscillatory characteristics of model compared with military requirements for satisfactory aircraft handling qualities.

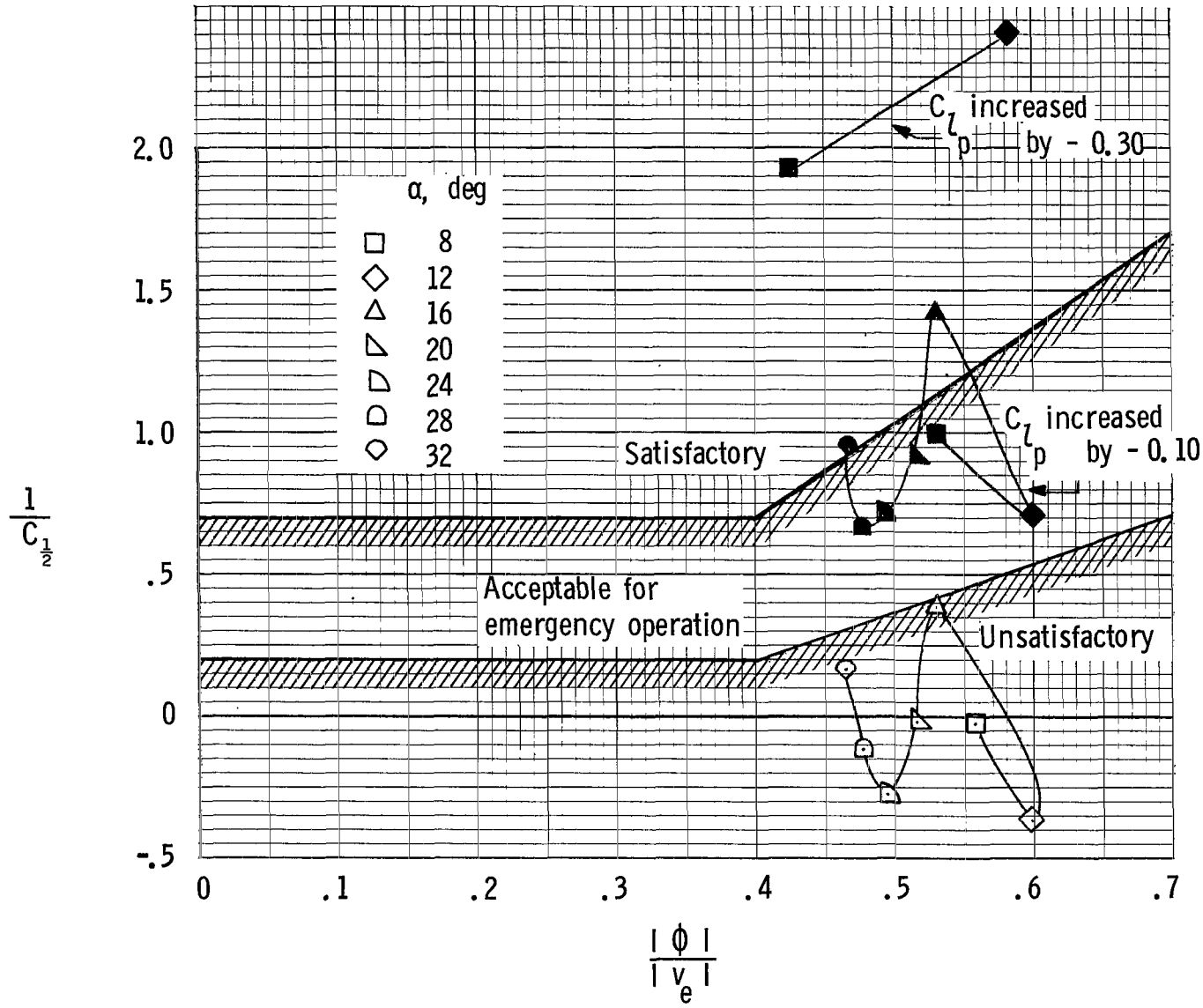

(b) Canard on (2-percent).

Figure 23.- Concluded.

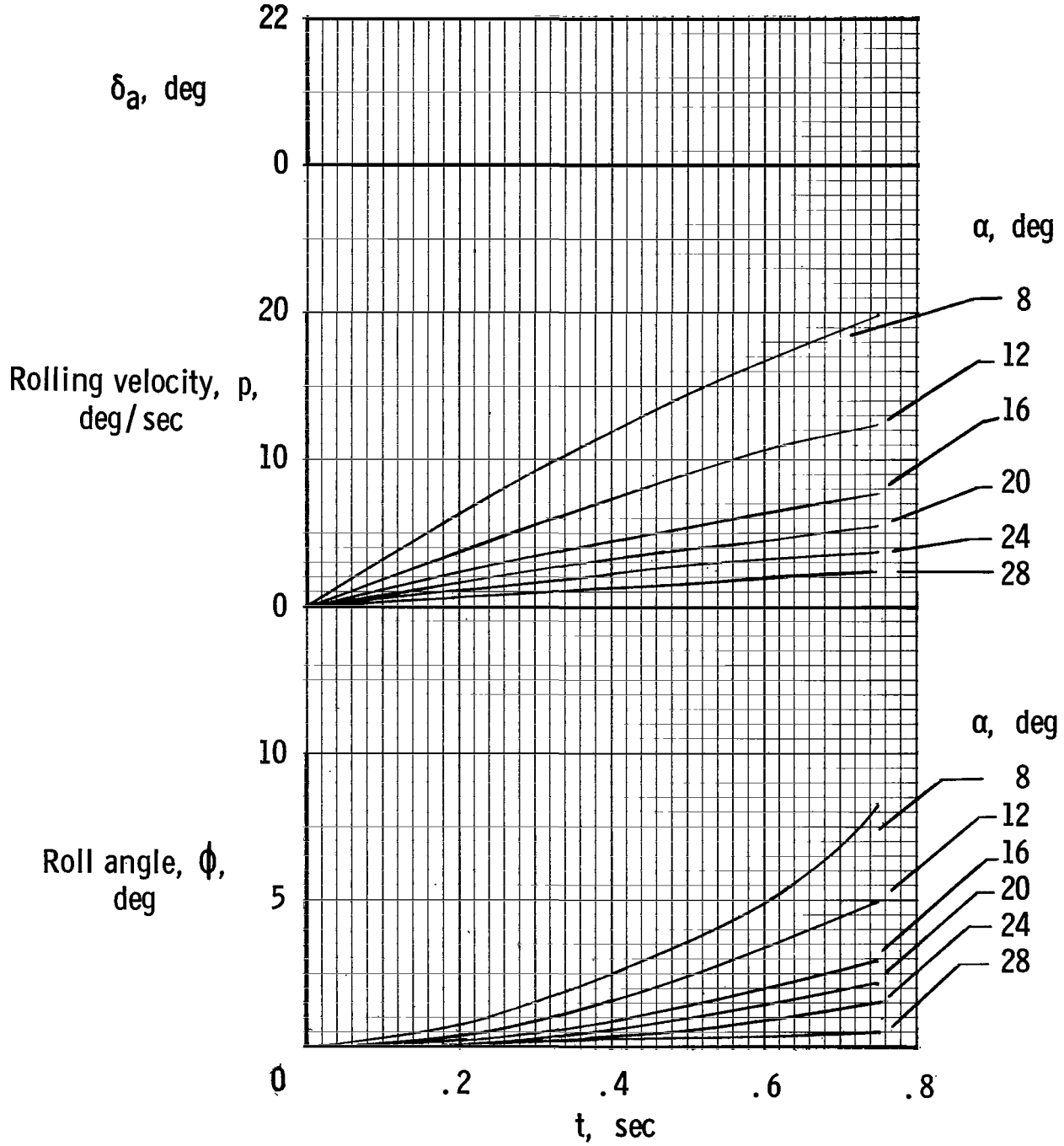

Figure 24.- Calculated full-scale single-degree-of-freedom roll-control response. Calculations based on measured force-test data of present investigation. Trailing-edge extension; notch; and leading-edge flaps.

"The aeronautical and space activities of the United States shall be conducted so as to contribute . . . to the expansion of human knowledge of phenomena in the atmosphere and space. The Administration shall provide for the widest practicable and appropriate dissemination of information concerning its activities and the results thereof."

—NATIONAL AERONAUTICS AND SPACE ACT OF 1958

NASA SCIENTIFIC AND TECHNICAL PUBLICATIONS

TECHNICAL REPORTS: Scientific and technical information considered important, complete, and a lasting contribution to existing knowledge.

TECHNICAL NOTES: Information less broad in scope but nevertheless of importance as a contribution to existing knowledge.

TECHNICAL MEMORANDUMS: Information receiving limited distribution because of preliminary data, security classification, or other reasons.

CONTRACTOR REPORTS: Scientific and technical information generated under a NASA contract or grant and considered an important contribution to existing knowledge.

TECHNICAL TRANSLATIONS: Information published in a foreign language considered to merit NASA distribution in English.

SPECIAL PUBLICATIONS: Information derived from or of value to NASA activities. Publications include conference proceedings, monographs, data compilations, handbooks, sourcebooks, and special bibliographies.

TECHNOLOGY UTILIZATION PUBLICATIONS: Information on technology used by NASA that may be of particular interest in commercial and other non-aerospace applications. Publications include Tech Briefs, Technology Utilization Reports and Notes, and Technology Surveys.

Details on the availability of these publications may be obtained from:

SCIENTIFIC AND TECHNICAL INFORMATION DIVISION

NATIONAL AERONAUTICS AND SPACE ADMINISTRATION

Washington, D.C. 20546